Description and validation of an AOT product over land at the 0.6 μm channel of the SEVIRI sensor onboard MSG

E. Bernard, C. Moulin, D. Ramon, D. Jolivet, J. Riedi, J.-M. Nicolas

Atmos. Meas. Tech., 4, 2543–2565, 2011
www.atmos-meas-tech.net/4/2543/2011/
doi:10.5194/amt-4-2543-2011

Atmospheric Measurement Techniques

Description and validation of an AOT product over land at the 0.6 µm channel of the SEVIRI sensor onboard MSG

E. Bernard[1,2], **C. Moulin**[2], **D. Ramon**[1], **D. Jolivet**[1], **J. Riedi**[3], **and J.-M. Nicolas**[4]

[1]HYGEOS, Euratechnologies, 165 avenue de Bretagne, 59000 Lille, France
[2]Laboratoire des Sciences du Climat et de l'Environnement, UMR8212, CEA-CNRS – Université de Versailles Saint-Quentin, Gif-sur-Yvette, France
[3]Laboratoire d'Optique Atmosphérique, UMR8518, CNRS, Université de Lille 1 – Sciences et Technologies, Lille, France
[4]ICARE Data and Services Center, Université de Lille 1 – Sciences et Technologies, Lille, France

Received: 15 April 2011 – Published in Atmos. Meas. Tech. Discuss.: 24 May 2011
Revised: 5 November 2011 – Accepted: 9 November 2011 – Published: 25 November 2011

Abstract. The Spinning Enhanced Visible and InfraRed Imager (SEVIRI) aboard Meteosat Second Generation (MSG) launched in 2003 by EUMETSAT is dedicated to the Nowcasting applications and Numerical Weather Prediction and to the provision of observations for climate monitoring and research. We use the data in visible and near infrared (NIR) channels to derive the aerosol optical thickness (AOT) over land. The algorithm is based on the assumption that the top of the atmosphere (TOA) reflectance increases with the aerosol load. This is a reasonable assumption except in case of absorbing aerosols above bright surfaces. We assume that the minimum in a 14-days time series of the TOA reflectance is, once corrected from gaseous scattering and absorption, representative of the surface reflectance. The AOT and the aerosol model (a set of 5 models is used), are retrieved by matching the simulated TOA reflectance with the TOA reflectances measured by SEVIRI in its visible and NIR spectral bands.

The high temporal resolution of the data acquisition by SEVIRI allows to retrieve the AOT every 15 min with a spatial resolution of 3 km at sub-satellite point, over the entire SEVIRI disk covering Europe, Africa and part of South America. The resulting AOT, a level 2 product at the native temporal and spatial SEVIRI resolutions, is presented and evaluated in this paper.

The AOT has been validated using ground based measurements from AErosol RObotic NETwork (AERONET), a sun-photometer network, focusing over Europe for 3 months in 2006. The SEVIRI estimates correlate well with the AERONET measurements, $r = 0.64$, with a slight overestimate, bias $= -0.017$. The sources of errors are mainly the cloud contamination and the bad estimation of the surface reflectance. The temporal evolutions exhibited by both datasets show very good agreement which allows to conclude that the AOT Level 2 product from SEVIRI can be used to quantify the aerosol content and to monitor its daily evolution with a high temporal frequency. The comparison with daily maps of Moderate Resolution Imaging Spectroradiometer (MODIS) AOT level 3 product shows qualitative good agreement in the retrieved geographic patterns of AOT.

Given the high spatial and temporal resolutions obtained with this approach, our results have clear potential for applications ranging from air quality monitoring to climate studies. This paper presents a first evaluation and validation of the derived AOT over Europe in order to document the overall quality of a product that will be made publicly available to the users of the aforementioned research communities.

Correspondence to: J. Riedi
(jerome.riedi@univ-lille1.fr)

1 Introduction

Tropospheric aerosols which are solid or liquid particles suspended in the air (Junge, 1958; Whitby, 1976), have two origins: natural and anthropogenic. Natural aerosols are a consequence of the wind effect on the surface (desert and marine origins), the burning of biomass and in a small proportion, biochemical reactions (Charlson et al., 1987; Kettle and Andreae, 2000). In addition, significant quantities of anthropogenic aerosols are emitted in the atmosphere. These

are mainly produced by the industrial activities, but also the agriculture, and once again biomass burning.

Aerosol effects on climate are dual: direct and indirect (Hansen et al., 2000). In the shortwave domain (0.3–4 µm), the direct "parasol effect" (Crutzen et al., 2003) leads to a decrease of the temperature beneath an aerosol layer covering the surface by reflecting the incident solar radiance; the temperature of the layer of the atmosphere where aerosols are located is increased by aerosol absorption of incident solar radiation. In the thermal infrared domain (8–15 µm), radiation emitted from the Earth is partly absorbed by aerosols and some is reemitted toward the ground, increasing both the aerosol layer and the underlying atmosphere and surface temperatures. This last phenomenon is especially important in case of absorbing aerosols. The indirect effect (Albrecht, 1989; Twomey, 1991; Lohmann and Feichter, 2005) is the increase of the condensation nuclei generation. The origin of the cloud formation being the presence in the atmosphere of cloud condensation nuclei (CCN) around which water vapour condensates, an increase of CCN can therefore affect cloud microphysics and consequently cloud physics (formation, evolution, dissipation) (Denman et al., 2007; Haywood and Boucher, 2000; Schwartz and Slingo, 1995; Hegg et al., 1993). These first and second indirect effects are currently a source of major uncertainties in cloud and climate models (Ghan et al., 2001; Hansen et al., 1997; Quaas et al., 2008; Schulz et al., 2006; Lohmann et al., 2010).

The direct radiative forcing due to aerosols is globally negative ($-0.5\,\mathrm{W\,m^{-2}}$ with the 5th and 95th percentiles at respectively $-0.1\,\mathrm{W\,m^{-2}}$ and $-0.9\,\mathrm{W\,m^{-2}}$, Forster et al., 2007) and the first indirect effect (also called cloud albedo effect or Twomey effect) generates a decrease of the radiative forcing estimated at $-0.7\,\mathrm{W\,m^{-2}}$ with the 5th and 95th percentiles at respectively $-0.3\,\mathrm{W\,m^{-2}}$ and $-1.8\,\mathrm{W\,m^{-2}}$ (Forster et al., 2007), but again these numbers remain highly uncertain. The knowledge of microphysical parameters of tropospheric aerosols and their distribution are therefore critical for the understanding of their effects on climate (Charlson et al., 1992; King et al., 1999) and the consequences on ground and atmosphere temperatures.

Another important issue related to aerosols monitoring is the relation existing between aerosols and air quality, especially in urban areas (Health Effects Institute, 2000; Lim et al., 2004; Sifakis, 1998). The air quality domain is the study of gas (CO_2, O_3, NO_x, ...) and solid particles called particulate matter (PM). Many studies in particular have tried to link the aerosol optical thickness (AOT) with the PM (Koelemeijer et al., 2006; Chu et al., 2003; Emili et al., 2010; Rohen et al., 2011; Wang and Christopher, 2003). For these applications, the monitoring of aerosol loading at a high temporal resolution is important. For the anthropogenic aerosols and near the sources of emission, the characteristic time of their presence in the atmosphere is typically of one hour and the spatial variation is around 1 km (Seinfeld and Pandis, 1997; Wayne, 2000). The meteorological conditions have a great influence on the stagnation and transport of an aerosol plume. Rapid variations could be detected with the high temporal resolution of SEVIRI. Grosso et al. (2007), for example, insist on the complementarity between ground air quality monitoring networks which are limited in terms of spatial coverage and satellite images which cover local and regional zone.

The detection of aerosols and the study of their evolution are difficult because of their low radiative signal, their rapid temporal evolution, their interactions with molecular gases and their regional variability.

Aerosols can be detected via an estimation of their optical thickness from the surface using ground-based sun photometers such as those from the AErosol RObotic NETwork (AERONET) (Holben et al., 1998), or using airborne and spaceborne instrumentation. Knowledge about aerosol impacts on the environment has increased significantly with the observation from space thanks to the provision of a global coverage, long term monitoring and a good characterization of physical aerosol parameters. Several global aerosol products over land are readily available from various sensors on polar orbiting satellites such as MODIS, MERIS, MISR, AVHRR, POLDER, TOMS and OMI (King et al., 1999; Mishchenko et al., 2007; Kaufman et al., 2002). If these Low Earth Orbiting (LEO) satellites can deliver rather high spatial resolution observations (around 1 km for the most of), the derived aerosol products are usually provided on a daily basis at a resolution of the order of ten kilometers or lower (MODIS or TOMS for instance). From geostationary satellites the surface sampled daily is for obvious reasons limited to the geostationary orbit field of view and the observations spatial resolution tends to be usually lower compared to instruments of the same generation on polar orbits, to a few exceptions such as OMI. However the high temporal resolution is an asset with a view to monitor the diurnal cycle of the aerosol load. Another advantage is the possibility to obtain more than 2 retrievals per day to increase the confidence in daily or monthly products. The capability to retrieve aerosol properties from a geostationary platform and monitor their diurnal cycle has been demonstrated by Knapp (2002) and Knapp et al. (2002, 2005), using the GOES sensor. Several aerosol studies over ocean have been performed also using the Meteosat first generation satellites (Moulin et al., 1997) and the Meteosat Second Generation (MSG) (Thieuleux et al., 2005).

MSG, launched by EUMETSAT, is on geostationary orbit since 2003 above the Guinea Gulf and the data are available in near-real time since this date every 15 min. Thanks to its position, the satellite is optimized to study the African, European and East of the South American continents, the Atlantic ocean and Mediterranean sea. The SEVIRI instrument is composed by 3 channels in the visible and near infrared (NIR) and 8 in the thermal infrared with a spatial resolution at sub-satellite point of 3 km and a High Resolution Visible (HRV) broadband channel with a spatial resolution of 1 km at sub-satellite point. The level 1.5 data available have been

corrected from radiometric and geometric non-linearity, geolocated and calibrated (Muller, 2007).

Recent investigations have used the Spinning Enhanced Visible and InfraRed Imager (SEVIRI) sensor onboard MSG to retrieve AOT over land in the visible channel centred at 0.6 µm and noted VIS06 in the following (Popp et al., 2007; Guerrieri et al., 2007; Carrer et al., 2010; Wagner et al., 2010). All these studies showed the feasibility of retrieving the AOT at time-scales ranging from 15 min (Popp et al., 2007; Guerrieri et al., 2007) to daily means (Carrer et al., 2010; Govaerts et al., 2010; Wagner et al., 2010).

Our algorithm (Jolivet et al., 2006; Bernard et al., 2009) is based on the assumption that the top of the atmosphere (TOA) reflectance in the VIS06 channel increases with the aerosol load (Fraser and Kaufman, 1985; Kaufman et al., 1997). After TOA reflectances have been corrected from gaseous and molecular contributions, the variable solar geometries combined with fixed viewing angle allow some angular sampling of the surface Bi-directional Reflectance Distribution Function (BRDF) and/or of the aerosol phase function. The algorithm developed aims to retrieve the AOT in the VIS06 channel in two steps using a method similar to the one developed for GOES-8 by Knapp et al. (2005). Over land, from a set of 14 days images, a map of estimated surface reflectance is built assuming that the darkest pixel for the period corresponds to a clean-sky observation (in fact the clearest). The second step is the retrieval of the AOT for each image using these surface reflectance maps and using a set of 5 aerosol models. The final product reports AOTs retrieved for each model along with an identification of the "best" estimate.

The algorithm generates maps every 15 min, that we validate against ground-based measurements (AERONET) for stations located in Europe. The study we present here concerns the validation of this aerosol land product over the Europe between March and July 2006. We also compare our product with data from the polar orbiting satellite Moderate Resolution Imaging Spectroradiometer (MODIS), onboard Aqua and Terra, and finally analyze limits of the algorithm and give future developments to improve the quality of the AOT product.

This paper is primarily intended at documenting the advantages and limitations of a first revision of an AOT product that will be made publicly available, knowing that identified problems are currently being investigated and improvements are being made. Therefore, instead of a detailed analysis of individual sources of error, we provide here an overall assessment of the product quality to allow potential users to develop their analysis with sufficient understanding about the product quality and validity range. Also, even though retrievals are performed over the full SEVIRI disk, this first evaluation of the product quality focuses over Europe where current retrievals are believed to have some virtues for the quantitative analysis of aerosol loading and diurnal evolution for air quality applications.

In Sects. 2 and 3, we first present the theoretical basis of an algorithm used to retrieve aerosol optical thickness from SEVIRI observations. Then, methodology and results of the validation of this product against AERONET ground based measurements are presented and discussed in Sect. 4. The capability of the SEVIRI product to follow the aerosol diurnal cycle is illustrated through cases study and discussed against AERONET and MODIS in Sects. 5 and 6. Finally, the daily mean AOT derived from SEVIRI is also compared to AERONET over 30 days periods and the comparison with daily maps of the level 3 MODIS is performed in Sect. 7. Conclusions and main findings are summarized in Sect. 8.

2 Surface-atmosphere modelling

If L (in $\mathrm{W\,m^{-2}\,sr^{-1}\,\mu\,m^{-1}}$) is the radiance measured at the top of the atmosphere, μ_s the cosine of the solar zenith angle and E_s the constant solar irradiance, the reflectance is given by:

$$\rho = \frac{\pi\, L}{\mu_s\, E_s}. \quad (1)$$

In clear-sky conditions, the TOA radiance derives from the contribution of the absorption and scattering by molecules and aerosols. Under some assumptions, we can dissociate three principal contributions and calculate them separately. First, for molecules, the absorption is independent from the scattering phenomenon. At the wavelength considered for our retrievals, 0.6 µm, the main gas which participates to the absorption is the Ozone. Regarding the scattering contribution, the molecules and aerosols are mixed in the atmosphere and a coupling effect appears. The radiance produced by such a coupling depends on many parameters: geometry, wavelength, surface pressure, aerosol type and aerosol optical thickness (Santer et al., 1999). Beyond 0.6 µm the coupling effect can be neglected (Ramon and Santer, 2001). In order to simplify the modelling, molecules and aerosols are separated and the Rayleigh scattering contribution is calculated separately. Therefore, the assumed atmospheric system consists of three separated layers: a molecular layer responsible for Rayleigh scattering, located above an aerosol layer and beneath a purely absorbing gaseous layer.

The surface is considered as a Lambertian reflector for surface-atmosphere coupling term. This last point is a simplification necessary to avoid expensive computational time. Indeed, a non-lambertian surface involves the coupling between the atmospheric directional downward radiation field with the BRDF of the target (Vermote et al., 1997b) which increases the complexity of the problem. This simple hypothesis could generate uncertainties in case of inhomogeous surfaces and important aerosol content (Vermote et al., 1997a).

Under all these assumptions, the top of the atmosphere reflectance for one wavelength is given by:

$$\rho_{\text{meas}}^{\text{TOA}}(\theta_S, \theta_V, \phi) = T_g \left[\rho_{\text{Ray}}(\theta_S, \theta_V, \phi) + \rho_{ag}(\theta_S, \theta_V, \phi) \frac{T_{\text{Ray}}(\theta_S, \theta_V)}{1 - \rho_{ag} S_{\text{Ray}}}\right] \quad (2)$$

where, T_g is the gas transmittance, ρ_{Ray}, and S_{Ray} are the reflectance and spherical albedo for the Rayleigh scattering, T_{Ray} is the Rayleigh transmittance for the downward and upward directions and ρ_{ag} is the reflectance at the top of the aerosol layer, also called the aerosol-ground reflectance. These quantities depend on the solar zenith angle (SZA) (θ_S), on the viewing zenith angle (VZA) (θ_V) and on the relative azimuth angle (RAA) (ϕ).

3 Description of the algorithm

From the native format data, the pixel counts of each channel are converted into radiances. Then, visible and near infrared channels are converted into reflectances from the Eq. (1) (Govaerts and Clerici, 2004) and brightness temperatures are computed for IR channels (IR3.9, IR8.7 IR10.8 and IR12) using the MSG reported calibration (EUMETSAT, 2007).

3.1 Cloud masking scheme

The first step in building the clear sky reflectance reference requires an identification of cloud covered or potentially cloud contaminated pixels. Although operational cloud masks exist, we are using a simpler yet efficient cloud masking scheme developed specifically for our application. The rationale for using a dedicated cloud mask is that it provides a handle on the cloud detection sensitivity. We can therefore allow for more or less cloud contamination in the first step of our algorithm and then refine the cloud masking at a later stage, either right after AOT retrieval, or during construction of level 3 products based on quality assurance flags set during the retrieval process.

Our cloud masking scheme is based on a two steps process during which we first try to classify pixels among four categories using an ensemble of thresholds based tests. Then, a temporal variability analysis on the High Resolution Visible and 10.8 µm channels is performed to refine the initial classification.

Taking example on the cloud mask developed for MODIS (Ackerman et al., 1998; Platnick et al., 2003) but adjusted to the spectral channels and spatial resolution of SEVIRI, our cloud mask is based on spectral thresholds and spatial coherence tests in the visible, near infrared and thermal infrared channels. The thresholds for the various tests have been set from detailed analysis of several scenes of SEVIRI images. As stated in Ackerman et al. (1998), the thresholds are never global but tend to represent as high a variety of situation as possible. However, the cloud detection scheme (hence the thresholds) is divided in an ocean and a land part because of the differences between the two types of surface reflectance magnitude in visible and near infrared spectral channels. The goal of each test is to estimate the probability of having a clear pixel (resp. a cloudy pixel). The value of a clear probability index (resp. a cloudy probability index) is increased if the test is achieved successfully. Finally, the respective values of both indexes determine the class of the pixel among four possible values: clear certain, clear uncertain, cloudy uncertain or cloudy certain. These cloud mask categories are respectively assigned a value of 0, 1, 2 or 3.

Note that we developed a cloud mask which does not depend on the availability of ancillary data such as meteorological reanalysis or forecast and does not require dynamic thresholds to be computed online using radiative transfer code as some more "evolved" cloud mask schemes sometimes do, so that the algorithm can be applied easily in a near real time environment using Eumetcast data dissemination system. Although this scheme appears rather simple compared to others, our cloud mask has proved to perform quite well and has been used with success for various studies (Roebeling et al., 2008).

In a second step, further tests using the high temporal resolution of the sensor are applied to the HRV channel and the IR108 channel (centred at 10.8 µm). The first one has a spatial resolution 3 times higher than the other channels and covers the visible wavelength region (0.37–1.25 µm). It improves particularly the discrimination between cloudy and clear pixels thanks to detection of small-scale features. We use the temporal information to detect the motion of clouds: over periods of 30 min (±15 min before and after the current SEVIRI image) temporal tests based on reflectance (HRV channel) or brightness temperature (IR108 channel) thresholds, allow to discriminate between 3 types of features: shadow, surface and cloud. The period can be extended to one hour (±30 min) when images do not exist in the database. The time scale is kept as low as possible (30 to 60 min) to limit the variation of the surface reflectance. Finally, a clear pixel identified in the first classification can be restored as cloud contaminated based on this temporal analysis.

3.2 Atmospheric corrections of level 1B

3.2.1 Gas absorption correction

Firstly, the absorption of the Ozone band in the VIS06 channel represents around 6 % of the TOA reflectance at nadir. A simple correction of this gas contribution is done assuming an angular dependence with the air mass, m ($m = \frac{1}{\mu_s} + \frac{1}{\mu_v}$) with μ_v the cosine of the viewing zenith angle. We also assume that the atmospheric quantity of Ozone is constant in time and uniformly mixed in the atmosphere. We consider a US62 standard atmosphere model with a quantity of 344 Dobson Units and the corresponding transmittance ($T_{0_3} = 0.94244$) for an air mass of 1 ($m_0 = 2$) as it is used in

Table 1. Physical and optical parameters of the aerosol models used in the algorithm (Omar et al., 2005).

♯		mode	R_v^5 (µm)	σ_v^6 (dV/dln$r$) [µm^3/µm^2]	V_o^7	n^8	F^9
1	WMO	–	–	–	–	–	–
2	MA[1]	Acc.	0.15	0.42	0.096	1.43–0.007i	0.82
		Coarse	3.26	0.77	0.092	1.43–0.007i	0.18
3	UI[2]	Acc.	0.18	0.43	0.096	1.42–0.007i	0.89
		Coarse	3.4	0.83	0.06	1.42–0.007i	0.11
4	SM[3]	Acc.	0.14	0.42	0.092	1.51–0.02i	0.91
		Coarse	4.0	0.76	0.064	1.51–0.02i	0.09
5	SD[4]	Acc.	0.14	0.76	0.087	1.48–0.0018i	0.83
		Coarse	2.2	0.55	0.068	1.48–0.0018i	0.17

Models are: [1] MA = Moderately Absorbing; [2] UI = Urban-Industrial non absorbing; [3] SM = Smoke; [4] SD = Spheroidal Dust. Number of each model is reported in the first column. The characteristics, given for both fine and coarse mode, are the median radius of the volume size distribution ([5]R_v) in µm, the neperian logarithm of [6]σ_v representing the standard deviation of this median radius, the volume of particles per cross section of the atmospheric column ([7]V_o) and the complex refractive index ([8]n) at 0.6 µm. The extinction fraction of each mode is also given ([9]F). The WMO continental model is from Lenoble and Brogniez (1984) (see text).

the 6S radiative transfer code (Vermote et al., 1997b). So, the transmittance is given by:

$$T_g = T_{0_3}^{\frac{m}{m_0}}. \quad (3)$$

From this, we get the reflectance at the top of the atmosphere corrected from the Ozone absorption as:

$$\rho_{meas}^{TOA,gas} = \frac{\rho_{meas}^{TOA}}{T_g}. \quad (4)$$

3.2.2 Rayleigh scattering correction

The reflectances are then corrected from the molecular scattering contribution in both visible channels (VIS06 and VIS08). The Rayleigh reflectance, transmittance and albedo are stored in Look-Up Tables (LUT's) calculated with the Successive Order of Scattering (SOS) radiative transfer code (Lenoble et al., 2007).

From the Eqs. (2) and (4), the TOA reflectance corrected from the Rayleigh scattering is calculated in two steps:

$$\rho_{meas}^{TOA*} = \frac{\rho_{meas}^{TOA,gas} - \rho_{Ray}}{T_{Ray}\ (\theta_S,\ \theta_V)} \quad (5)$$

then,

$$\rho_{ag} = \rho_{ag}^{meas} = \frac{\rho_{meas}^{TOA*}}{1 + S_{Ray}\ \rho_{meas}^{TOA*}}. \quad (6)$$

This reflectance is the result of the first step of the algorithm, called the level 1B (L1B).

3.3 Estimation of the surface reference reflectance

Once the first step is achieved, a set of (cloud free) aerosol-ground reflectances is available. Aerosol contribution is separated from ground contribution using Eq. (7):

$$\rho_{ag}^{sim} = \rho_{Aer} + \rho_g \frac{T_{Aer}}{1 - S_{Aer}\ \rho_g}. \quad (7)$$

The unknowns are the ground reflectance, ρ_g, and the 3 parameters which govern the scattering by aerosols: the reflectance (ρ_{Aer}), the spherical albedo (S_{Aer}) and the transmittance (T_{Aer}) in the upward and downward directions.

To derive the surface reflectance (ρ_g) over land, we assume that in a period of several days, the minimum of the aerosol-ground reflectance is the contribution of the surface and a residual aerosol load. As discussed previously, the method of the minimum is not valid above bright surfaces in the presence of absorbing aerosols (Kaufman et al., 1997). This point is discussed in Jolivet et al. (2006) showing that the TOA reflectance decreases with increasing AOT. So, the minimum reflectance found will not necessarily be the absolute TOA minimum reflectance which would occur under perfectly clean sky conditions.

Taking example on Knapp et al. (2002), a residual aerosol optical thickness of 0.03 (τ_{back}) is chosen considering the WMO continental model (see Table 1 for a description of the aerosol models). This assumption is globally realistic even if spatial and temporal variations of aerosols in the atmosphere and the spatial inhomogeneity of aerosol models should ideally be considered.

To determine the optimal period during which the reference reflectance should be looked for, a number of solar/satellite geometric considerations must be accounted for. During a 14 days period the SZA varies between 0.5° and

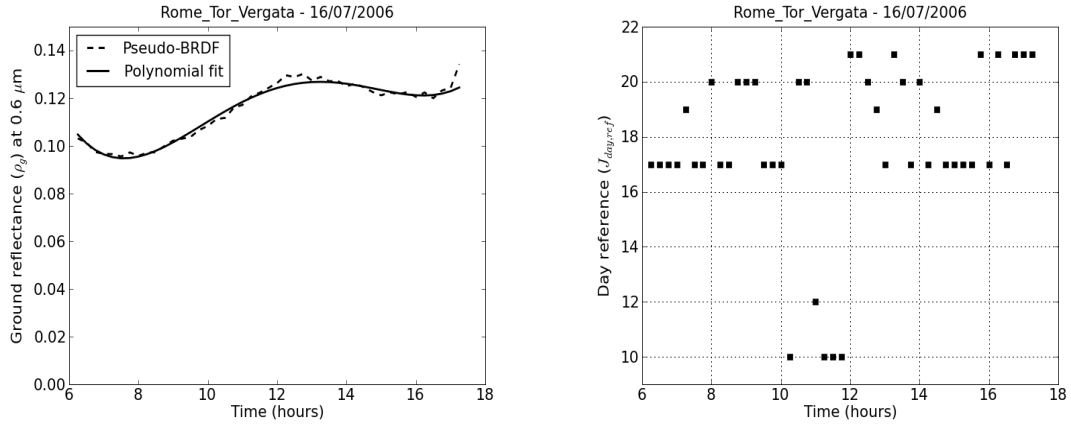

Fig. 1. Rome site on the 16 July 2006. Left panel: ground reflectance (ρ_g) at 0.6 µm: the subset of BRDF (or reference reflectance) based on the 14 days minimum (black dashed curve) and the fourth degree polynomial fit (black curve). Right panel: $J_{day,ref}$: the day with the smallest L1B reflectance at VIS06 channel.

1.5°, depending on the latitude, and the RAA varies between −1° and 4° for the same time of the day (Jolivet et al., 2006). These variations do not lead to significant changes of the ground reflectance. However, in case of "hot spot" geometry (due to the backscattering of the sunlight by foliage), when the scattering angle (angle between the solar and viewing directions) is close to 180°, rapid variation of the ground reflectance is observed. This situation occurs in Europe around the equinox.

We also assume that for such a period, surface properties (farmland, building constructions, forests, ...) do not change significantly. When we consider a shorter time range of 7 days, the number of pixels kept for the estimation of the reference reflectance is 20 % lower than for a 14 days period. For a longer period, this number does not increase significantly (Jolivet et al., 2006). A similar study (Knapp et al., 2005) determined a best period of 14 days to retrieve the surface reflectance from a geostationary platform (GOES). Note that Popp et al. (2007) chose a period of 31 days for their studies but for the reasons previously mentioned this longer period may induce some severe geometrical biases.

So for each pixel of a given image (J_{day}), the algorithm looks for the day with the smallest L1B reflectance in the VIS06 channel over 14 days and considers this particular day ($J_{day,ref}$) with a minimum of aerosol load (see Fig. 1). This procedure is applied to all pixels in order to construct a reference map of bi-directional reflectance valid for the scene and the time and day considered. The basis of the algorithm relies on identifying confident clear pixels so that building of this clear sky reference map is only done using "clear certain" pixels. Once every image of the day has been processed, we reconstruct the diurnal variation of the surface reflectance, for a fixed VZA (θ_v) and several SZA (θ_s).

This subset of BRDF is then temporally fitted with a fourth degree polynomial function to, on one hand, minimize the temporal noise due to the compositing method, and on the other hand, remove the potential positive bias caused by cloud contamination and negative bias introduced by cloud shadows. This surface reflectance is called the reference reflectance in the following of the text (Fig. 1).

Note also that the fit is weighted using a quality index, assigned to each pixel of every image. This index is based on several tests: pixels with no data, number of days use to find the minimum, temporal test on the presence of data and successive tests on the polynomial standard deviation. The quality index increases in case of the tests fail. The index values range from 0 (high confidence) to 10 (low confidence).

3.4 Description of level 2 processing

3.4.1 Basis for AOT retrieval

Once a reference reflectance for the surface has been established, the aerosol terms (ρ_{Aer}, T_{Aer}, S_{Aer}) in the Eq. (7) remain unknown.

We simulate these terms linked to aerosols using the SOS radiative transfer code (Lenoble et al., 2007) for a range of sensor and solar zenith and azimuthal angles and aerosol optical thicknesses (varying from 0 to 2.5 with a step of 0.05) for five aerosol models in the visible and NIR channels. These results are stored in LUT's for use during the retrieval process.

Among the five aerosol models used, four are from Omar et al. (2005): moderately absorbing (MA), urban-industrial (UI), smoke (SM) and spheroidal dust (SD) (spherical shape is used to simplify calculation). They have a two-modes (accumulation and coarse modes) log-normal size distribution and their optical and geometrical features are given in Table 1. This distribution is based on the median radius: few 10^{-1} µm for the coarse mode and between 5×10^{-3} µm and 10^{-2} µm for the fine mode. Parameter F gives these proportions (Table 1). In addition, a fifth model from the World

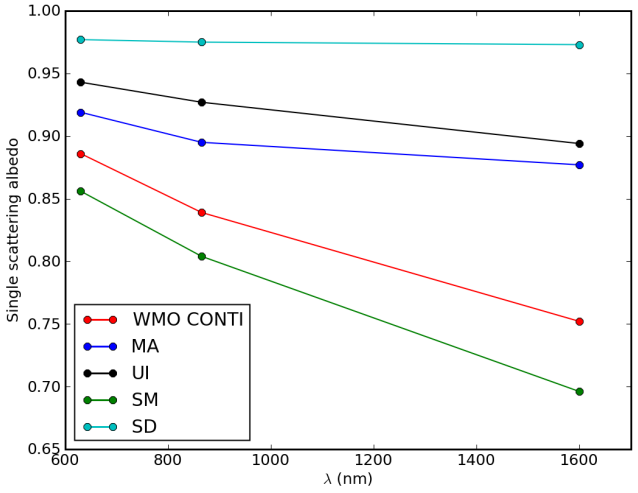

Fig. 2. Single scattering albedo (ϖ_0) for the 5 aerosol models used by the algorithm to retrieve the AOT at 0.6 µm.

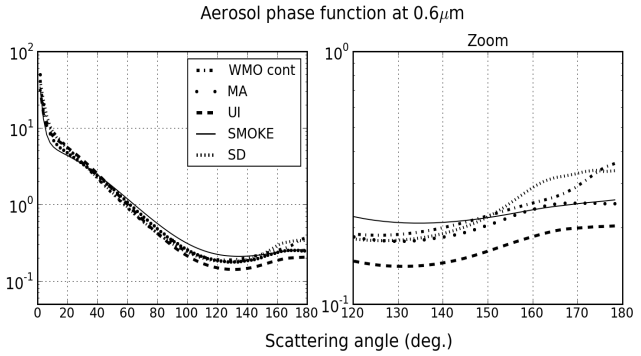

Fig. 3. Aerosol phase function for each 5 models at 0.6 µm between 0° and 180° (left panel). A zoom for the backscattering part (from 120° to 180°) is also plotted (right panel).

Meteorological Organization (WMO) (Lenoble and Brogniez, 1984) is used, identified as a continental model (WMO cont), and composed of a proportion of three components: dust-like, water-soluble and soot, respectively in these proportions: 70 %, 29 % and 1 %. In the same manner for models from Omar et al. (2005), we separated into two modes this WMO continental model with 91 % for the accumulation mode and 9 % for the coarse mode.

The single scattering albedo of each model is plotted in Fig. 2. Three groups could be distinguished: a nearly non-absorbing model (SD), $\varpi_0 = 0.98$, a moderately absorbing group (MA + UI): $0.88 < \varpi_0 < 0.95$, and an absorbing group (WMO cont + SM): $0.9 < \varpi_0 < 0.7$. The phase function in the VIS06 channel of each model is also plotted (see Fig. 3).

Using ρ_g, the aerosol/ground reflectance can be computed in the VIS06 channel (Eq. 7) by adjusting for each aerosol model the AOT to match the Rayleigh and gas corrected measured reflectance (ρ_{ag}^{meas} in Eq. 6). Then, the aerosol/ground reflectances (Eq. 7) in the VIS08 and NIR16 channels (centred at respectively 0.8 µm and at 1.6 µm) are derived directly from the LUT's for each aerosol model. Finally, the algorithm discriminates between the aerosol models and selects the best estimate by minimisation of the square difference between $\rho_{ag_\lambda}^{sim}$ and $\rho_{ag_\lambda}^{meas}$ with $\lambda = 0.8$ and 1.6 µm. Note that the product actually reports the AOT values retrieved in the VIS06 channel for all five models. The identification of the so-called best estimate is done in an attempt to fully use the potential of SEVIRI spectral capabilities. However, we currently have limited understanding of the spectral coherence of inter-channel calibration and therefore, the information carried by the best-estimate model shall not be overestimated and in particular does not represent, at this stage, an absolute determination of the aerosol type on a individual pixel basis. However, this information can again be used at a later stage during level 3 construction or during diurnal evolution analysis to enforce respectively some spatial or temporal coherence in the product.

This procedure is applied on each individual pixel identified as clear by the cloud mask scheme ("clear certain" and "clear uncertain").

For obvious reasons, retrieval is attempted only for pixels under daylight conditions and bright surfaces are discarded for reasons already developed in Sect. 3.3. The bright surfaces are essentially desert areas (Sahara, Sahel, Namib) where the Rayleigh and Ozone corrected VIS06 TOA reflectance is approximately greater than 0.25. Also, for the same reason, retrieval is performed only when the measured aerosol ground reflectance ρ_{ag} is greater than the reference ground reflectance ρ_g in the VIS06 channel.

For development purposes only and to help in identification of discontinuity problems over land, we also retrieve the AOT over ocean using a similar approach and a simplified representation of the ocean surface. Over ocean, the target is dark and the spatial and temporal variability of the reflectance is low compared to land. Thus, the main contribution to the TOA reflectance is the atmosphere and the reflectance of the water is negligible as explained in Thieuleux et al. (2005) except near coasts and for sun-glint configurations. The difference with the ocean algorithm of Thieuleux et al. (2005) is that we assume a very low reflectance for the water. These values are: 2×10^{-3} for the VIS06 channel, 1×10^{-4} in the VIS08 channel and 1×10^{-5} in the NIR16 channel. Again, this over simplified approach only serves the purpose of checking the continuity in retrieved AOT between ocean and land.

The product is finally provided over the entire SEVIRI disk every 15 minutes between 05:00 and 19:45 UTC.

3.4.2 Quality assurance filters

As previously explained, the level 2 aerosol product is retrieved over the entire SEVIRI disk. However, all pixels are not directly usable because they may correspond to

undetected thin clouds or cloud edges, or extreme observation geometries that usually lead to doubtful retrievals. A quality assurance mask is constructed and provided with the product to identify such situations where the aerosol inversion could be doubtful.

First of all, pixels under high viewing angles or low illumination conditions could be considered as doubtful because several assumptions made by the 6S and SOS radiative transfer developments fail under these particular geometrical conditions. Indeed, the assumption of two separated scattering layers (aerosol + molecule) used here and valid in 6S development, falls short when the solar or viewing angles are greater than 70°. In these conditions, coupling effects between aerosol particles and molecule start to be significant and Eq. (2) does not apply anymore.

As discussed in Sect. 3.3, the "hot spot" configuration leads to an under-estimation of the surface reflectance, due to the polynomial fit, and so, to an over-estimation of the aerosol reflectance. This scenario occurs for scattering angles close to 180° and in general is identified as a doubtful reference estimation pixel with an index reference greater than 4. But, the exact value of the limit angle is unclear. So, we use a rather strict upper limit of 170° scattering angle to avoid even the most difficult cases.

In addition, a test based on the local standard deviation of the AOT (σ_τ) is done and three classes are identified: $\sigma_\tau \leq 0.05$, $0.05 < \sigma_\tau \leq 0.1$ and $\sigma_\tau > 0.1$. Isolated pixels have a $\sigma_\tau = 0$ and are identified as such in the Quality Assurance flag so that they can later be rejected. This test is applied on ensembles of 3 by 3 pixels and aims at removing spurious AOT values caused by presence of cloud edges or thin clouds. This relies on the assumption that spatial variability of retrieved AOT will be greater for a region partly contaminated by undetected clouds compared to only aerosols due to the more continuous nature of aerosol layers.

4 Evaluation of the level 2 product

4.1 AERONET data

The validation is performed against ground-based sunphotometers measurements of the international AERONET (Holben et al., 1998) network. We used the level 2 quality assured AOT product at 675 nm. We focused the validation over the Europe for three months in 2006 (March, April and July), and selected 43 stations (see Table 2) for which aerosol optical thickness is available for at least one month.

4.2 Filtering the level 2 product

We use the information of the quality assurance mask to filter the level 2 aerosol optical thickness and keep the most confident pixels to compare with measurements from the ground.

Observations corresponding to scattering angles greater than 170° are discarded and pixels viewed or illuminated under an angle greater than 70° are also rejected. Only pixels declared by the cloud mask as "clear certain" are kept for the validation to minimize contamination by potentially remaining undetected clouds.

A selection of the most confident reference reflectance pixels is done. In a general way, the relative offset between the subset of BRDF and the temporal fit is between 1 % and 5 %. A few exceptions occur at the start or the end of the day with some biases reaching 20 %. We remove pixels with a reference quality index above 3.

We choose to keep non isolated pixel with a local aerosol standard deviation (σ_τ) lower than 0.1

4.3 Validation of the level 2 product

We present here results for the filtered AOT product over land and compare it with the AOT measured at 675 nm by AERONET. The SEVIRI pixel used for the validation is the one geolocated with the AERONET station. The AERONET AOT value is obtained by temporally averaging all retrievals available ±10 min around the SEVIRI observation time.

Figure 4 shows the comparison between SEVIRI and AERONET AOT for the 3 months together and each months separately. With a total of 5637 match-up (N) the agreement between AERONET and SEVIRI is good with a correlation coefficient of 0.64 and a linear regression with a slope of 0.8 and an intercept of 4×10^{-2}. The negative bias (AERONET-SEVIRI) of -0.017 denotes a low but global over-estimation of the AOT by the SEVIRI retrievals. This bias is between -0.03 and 0.007 for AOT < 0.3 and from 0.02 to 0.15 for AOT ≥ 0.3. Note that the number of match-up decreases with increasing AOT, with N reaching 5515 for AOT < 0.3 and only 122 for AOT $\geq$0.3.

The mean relative error for AOT < 0.1 is high (63 %) and very low (<5 %) for AOT ≥ 0.1. As can be seen on the density graph (Fig. 4) the bulk of the match-up is very close to the unit curve. The error is of the same order of magnitude as the estimation of the aerosol background (τ_{back}) for low AOT with a high number of correlation points. Then, the number of match-up and the error are low for high AOT.

The rather high value of the root mean square error (RMSE) (close to 0.07) traduces a large dispersion for both low and high AOT. Over-estimated SEVIRI AOTs are likely due to cloud contaminated pixels which are not detected by the cloud mask and not removed by the filtering tests. Under-estimated AOTs by SEVIRI are related to the under-estimation of the background aerosol load. Also, errors on the estimate of the reference surface reflectance directly lead to an over or under estimation of AOT. Such errors are caused mostly by the temporal fit that we apply to smooth the diurnal variation of surface reference which tends to introduce systematic biases in case of local non-uniform surface configurations such as mountain slopes.

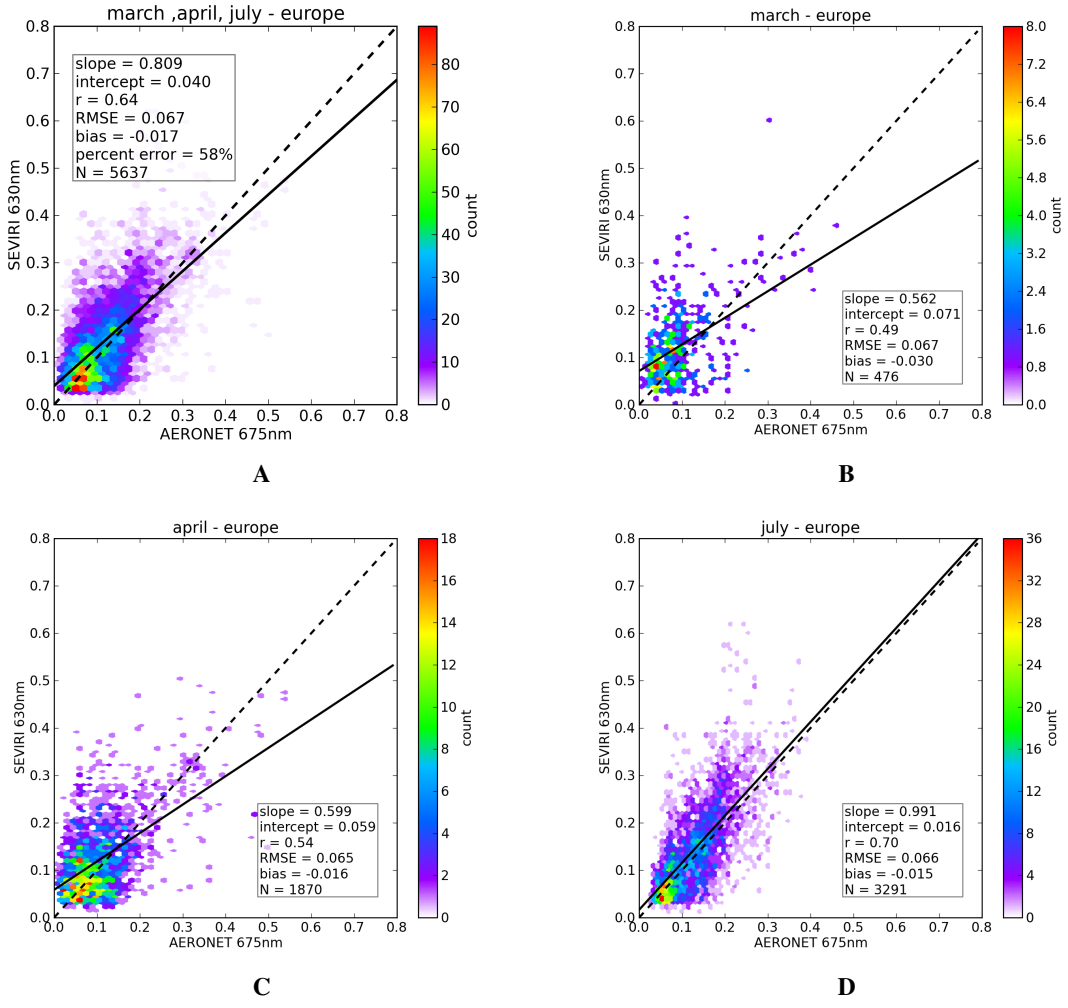

Fig. 4. Density graph of AOT SEVIRI against AERONET at 0.6 µm for European stations for the 3 months: March, April and July 2006 **(A)**. The linear regression (black line) and the one-to-one curve (black dashed line) are plotted. The parameters of the linear regression are indicated on the graph. Individual validation for the 3 months separately are also plotted: March **(B)**, April **(C)** and July **(D)**.

The results of the linear regression for July are the best: a correlation coefficient of 0.7, a slope of 0.9 and a low intercept (0.016). Consistent AOT up to 0.4 are retrieved in comparison with AERONET. Every station gives satisfying correlations except for Belsk and Chilbolton for which a large number of points over-estimate AOT compared to ground-based measurements. For April, the number of match-up is about 4 times greater than for March but the parameters of the linear regression are approximately the same and only the bias gets improved (divided by 2). We observe high consistent values between 0.3 and 0.6 for April. The RMSE is the same for each months so denotes a constant dispersion from the measurements regardless of the month considered.

March suffers from various problems. It is a cloudy month for Europe with a limited number of clear days available for construction of the reference (476 in March and 3291 in July). Secondly, the set of level 1 data is low: from the 2 to 5 March 2006 there is no data, and some days suffer from a lack of images. For the first period of the month, the data set among which the minimum of the TOA reflectance is looked for, is reduced from 14 days to less than 10 days (lack also of the 27 and 28 February). So, it reduces significantly the chance to observe a given pixel under clear conditions. For March, and generally for cloudy periods or periods with an important lack of raw data, a longer period of investigation to retrieve a clear day could be necessary. All these factors contribute to negatively impact the quality of our surface reflectance reference.

A bias is found for March which is twice that of the two other months. This is explained by a more important number of over-estimated data which could be due to the failure of the cloud mask or/and to a problem in the estimation of the reference reflectance. A strong link obviously exists between the cloud detection and the construction of a good reflectance reference and our cloud mask scheme could certainly be improved. However, over-estimation of the AOT could be due

Table 2. Coordinates and description of the 43 AERONET stations used for the validation.

Stations	Lat.	Lon.	Stations	Lat.	Lon.
Avignon (FR.[1])	43.9° N	4.88° E	La Crau (FR.[1])	43.58° N	4.8° E
Barcelona (ES.[4])	41.39° N	2.12° E	Laegeren (CH.[10])	47.48° N	8.35° E
Belsk (PL.[12])	51.84° N	20.79° E	Lecce University (IT.[8])	40.33° N	18.11
Brussels (BE.[9])	50.78° N	4.35° E	Le Fauga (FR.[1])	43.38° N	1.28° E
Cabauw (NL.[11])	51.97° N	4.93° E	Lille (FR.[1])	50.61° N	3.14° E
Cabo Da Roca (PT.[3])	38.78° N	9.5° W	Mainz (DE.[2])	50° N	8.3° E
Carpentras (FR.[1])	44.08° N	5.06° E	Minsk (BY.[16])	53.92° N	27.6° E
Chilbolton (UK.[17])	51.14° N	1.44° W	Modena (IT.[8])	44.63° N	10.94° E
Davos (CH[10])	46.8° N	9.84° E	Moldova (MD.[7])	47° N	28.81° E
Dunkerque (FR.[1])	51.03° N	2.37° E	Moscow MSU MO (RU.[6])	55.7° N	37.51° E
Epanomi (GR.[5])	40.37° N	22.98° E	OHP Observatory (FR.[1])	43.93° N	5.7° E
Evora (PT.[3])	38.57° N	7.9° W	Oostende (BE.[9])	51.22° N	2.92° E
Fontainebleau (FR.[1])	48.4° N	2.68° E	Palaiseau (FR.[1])	48.7° N	2.2° E
Forth crete (GR.[5])	35.33° N	25.28° E	Palencia (ES.[4])	41.99° N	4.51° W
Granada (ES.[4])	37.16° N	3.6° W	Paris (FR.[1])	48.87° N	2.33° E
Hamburg (DE.[2])	53.57° N	9.73° E	Rome Tor Vergata (IT.[8])	41.84° N	12.65° E
Helgoland (DE.[2])	54.18° N	7.89° E	Sevastopol (UA.[13])	44.61° N	33.52° E
IMAA Potenza (IT.[8])	40.6° N	15.72° E	SMHI (SE.[14])	58.58° N	16.15° E
Ispra (IT.[8])	45.8° N	8.63° E	Thessaloniki (GR.[5])	40.63° N	22.96° E
The Hague (NL.[11])	52.11° N	4.33° E	Toravere (EE.[15])	58.25° N	26.46° E
Toulon (FR.[1])	43.14° N	6° E	Venise (IT.[8])	45.31° N	12.5° E
Villefranche (FR.[1])	43.98° N	7.33° E			

The country of each station is indicated in parenthesis: [1] FR. = France, [2] DE. = Germany, [3] PT. = Portugal, [4] ES. = Spain, [5] GR. = Greece, [6] RU. = Russia, [7] MD. = Moldova, Republic Of, [8] IT. = Italy, [9] BE. = Belgium, [10] CH. = Switzerland, [11] NL. = The Netherlands, [12] PL. = Poland, [13] UA. = Ukraine, [14] SE. = Sweden, [15] EE. = Estonia, [16] BY. = Belarus, [17] UK. = United Kingdom.

also to the under-estimation of the surface reflectance which in March could occur over Europe because of rapid change in vegetation cover. Finally, March is a period during which observations under the "hot-spot" configuration are the most common over Europe. The temporal fitting of the surface reflectance reference tends to smooth out this feature of the BRDF yielding a systematic under estimate of surface reflectance in this particular observation geometry. The limit value of 170° applied to the scattering angle may not be restrictive enough in some cases and could partly contribute to this general overestimate of AOT in March. Despite this, retrievals for March are acceptable for high AOTs up to 0.4.

The main interest of SEVIRI is the high temporal frequency of observation. To illustrate this, two particular stations are considered for which the diurnal evolution of the SEVIRI AOT is plotted and compared with AERONET measurements. Cabauw (Fig. 5) and Rome (Fig. 6) are located at the North and South of Europe, with different types of surface: Cabauw is in an agricultural region and Rome Tor Vergata is located in the suburb area of Rome.

A very good general monitoring is observed for both stations. The diurnal cycle is well reproduced by SEVIRI with an important number of retrievals per day. For Rome the daily mean absolute relative error (percent error) is between 20 % and 30 % and the bias is close to zero (0.003) except for the 14 on which SEVIRI over-estimates AERONET by 0.04. For Cabauw the relative bias ranges from 6 % to 58 %.

For instance, for Cabauw on 1 July 2006 (Fig. 5), the maximum, in the morning, and the minimum, in the afternoon, are well retrieved by SEVIRI. The two maxima at 13:30 and 14:30 are missing in SEVIRI retrievals because they have been rejected during cloud screening. On 2 July 2006, SEVIRI is in very good agreement with AERONET before 11:00 and after 13:00. Between these two hours, SEVIRI retrieves an aerosol optical thickness greater than 0.22 while AERONET measures an AOT of 0.15 at only two hours: 12:15 and 12:45. Visual inspection of the visible images during that timeframe revealed the presence of scattered clouds around the station which were probably too small to be detected with the spatial resolution of SEVIRI ($\simeq$5 km at this latitude).

In general, SEVIRI aerosol retrievals show a good stability of the AOT from one slot to the other except in some cases such as 20 July 2006 above Rome (Fig. 6). Between 11:00 and 14:00 the aerosol optical thickness varies between 0.1 and 0.2. From 11:15 to 11:45 the best aerosol model is successively the MA and the SM model, and the AOT varies between 0.06 (MA) and 0.2 (SM). This change

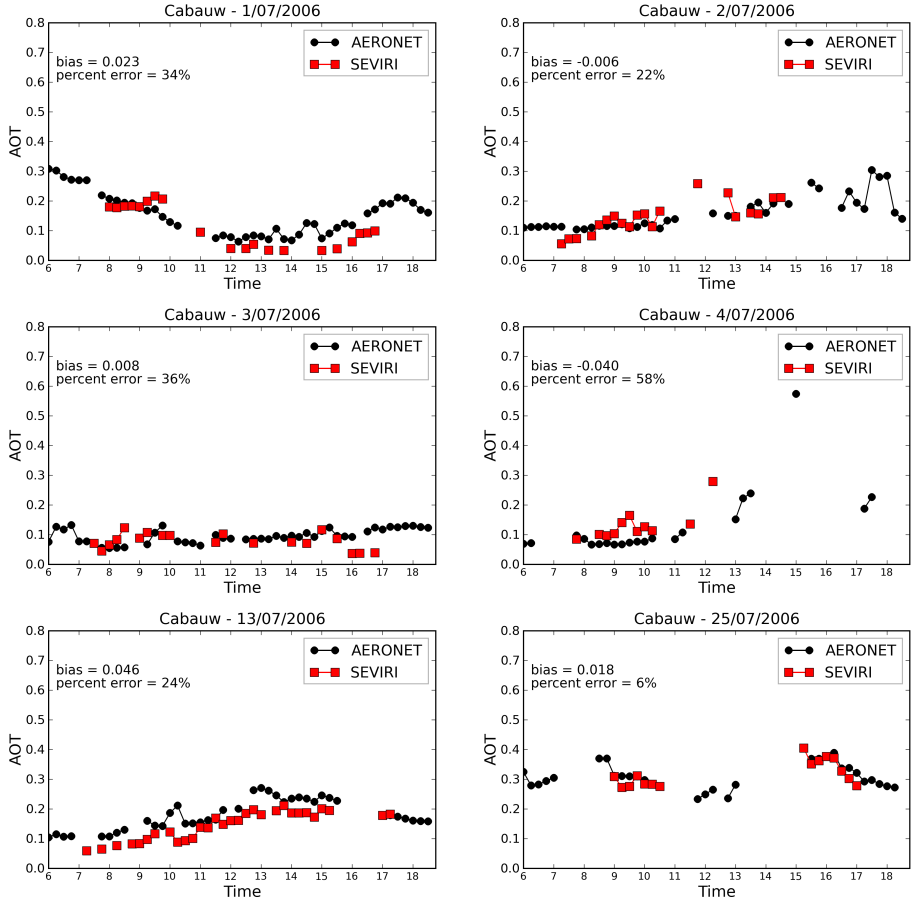

Fig. 5. Temporal evolution of the aerosol optical thickness above Cabauw for some days in July 2006: from 1 to 4 and on 13 and 25. The black line is AERONET and the red line is SEVIRI. The time scale is from 06:00 to 18:00 UTC and the AOT scale is from 0 to 0.7. The mean bias and the mean relative bias are indicated on each plot.

is explained by the method used to select the best model and the spectral characteristics of SEVIRI: the discrimination between the models is difficult and several models could match the measurements. Figure 7 shows the AOT retrievals for each model and for the best model for this particular day. The best model number is also plotted (see Table 1). At the beginning and at the end of the day, the differences between each model are very small and all of them match very well the measurements. Around midday, because of the geometrical conditions, these differences increase, but for this particular day and station, the AOT measurements remain in the range of AOT available through the 5 different models. Differences between AOT retrieved for each model is the consequence of the optical properties and particularly of their absorption properties. In the VIS06 channel the single scattering albedo ranges from 0.98 to 0.85 (Fig. 2).

These examples illustrate the unique potential of SEVIRI to observe the diurnal variability of AOT. The next Section shows that the rather good agreement of our product with AERONET is further confirmed when we compare with the large scale variability of AOT observed simultaneously by MODIS over Europe.

5 Monitoring of a particular aerosol event

In this Section we investigate AOT maps over France in July to show the spatial consistency of level 2 product at the original temporal resolution during an aerosol event.

On 14 July 2006, an important aerosol event is present all day long above the northern France and western Germany, with a mean AOT around 0.35–0.4 (Fig. 8). At that time of July 2006, there were active fires in both Spain and Portugal as well as some dust events coming from North Africa. The event we describe here seems predominantly associated with transport of biomass burning aerosols arising from the Iberian peninsula.

Two AERONET stations have recorded these high aerosol optical thicknesses: Fontainebleau and Palaiseau, both located near Paris (Fig. 9). SEVIRI AOT are well correlated to these measurements with a mean bias of 0.04 and −0.017. A third station in the south of France, Le Fauga, measured an AOT greater than 0.2 during the day with a maximum of 0.4 early in the morning (Fig. 9). SEVIRI has only 3 retrievals around midday which over-estimated AOT compared to AERONET. This could be due to scattered clouds that

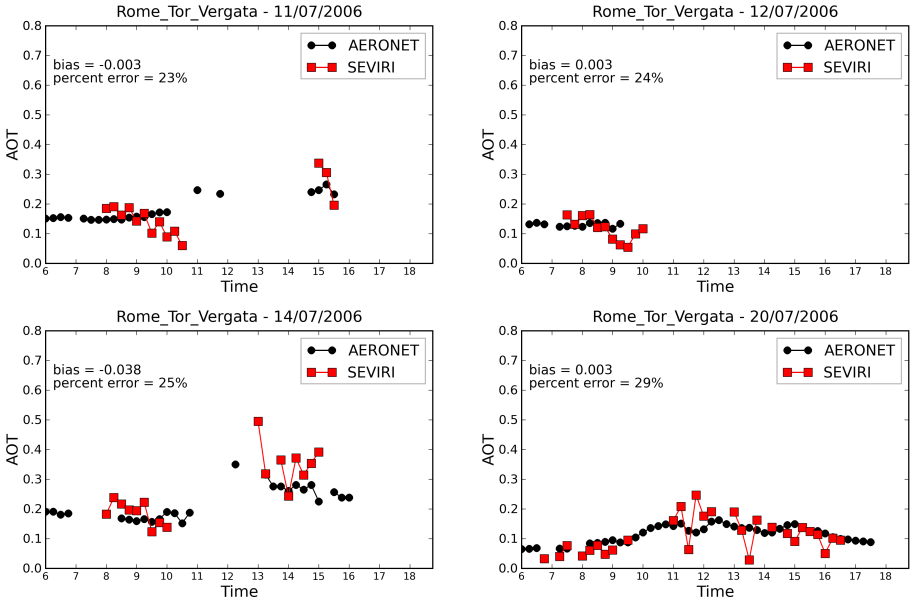

Fig. 6. Same as Fig. 5 but for Rome Tor Vergata station for days: 11, 12, 14 and 20 on July 2006.

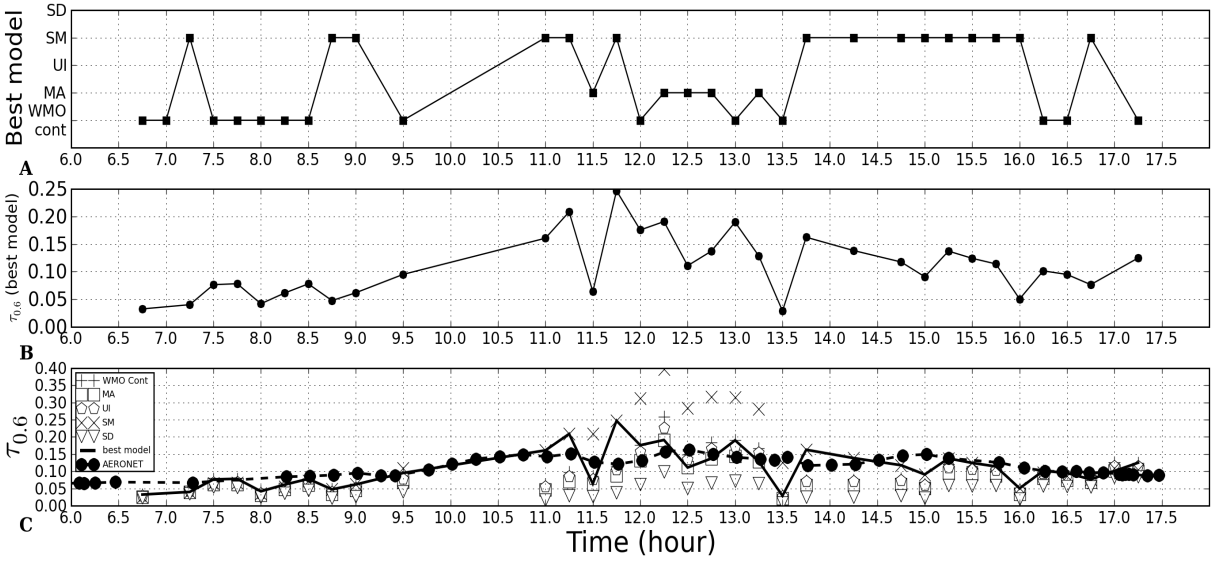

Fig. 7. Temporal evolution of aerosols parameters retrieved over Rome on the 20 July 2006. **(A)** Best aerosol model retrieved by the algorithm (see Table 1). **(B)** SEVIRI best model aerosol optical thickness at 0.6 µm. **(C)** Aerosol optical thickness for each model (symbol): WMO continental (plus), Moderatly Absorbing (square), Urban Industrial (pentagon), Smoke (cross), Spheroidal Dust (triangle). AOT best model (black line) and AOT AERONET (black circle).

cover the south of France and may affect the accuracy of the product (Fig. 8).

In the north of France and above Benelux, a very low aerosol optical thickness is retrieved, around 0.1, confirmed by 2 AERONET stations, Lille and Cabauw, with which SEVIRI is in good agreement (Fig. 9). Above Cabauw, SEVIRI retrieves AOT equal to 0.2 between 11:00 and 12:30 while AERONET measures AOT of 0.1. Once again, scattered clouds around the Cabauw station during that day may well be responsible for this bias, as suggested by the relatively high local standard deviation of the AOT which is close to the threshold of 0.1 (see Sect. 3.4.2).

Two successive Aqua overpasses on 14 July 2006 can be temporally matched with SEVIRI observations at 12:00 UTC and 13:45 UTC. MODIS aerosol products derived from granules acquired between 12:00 and 12:10, and between 13:45

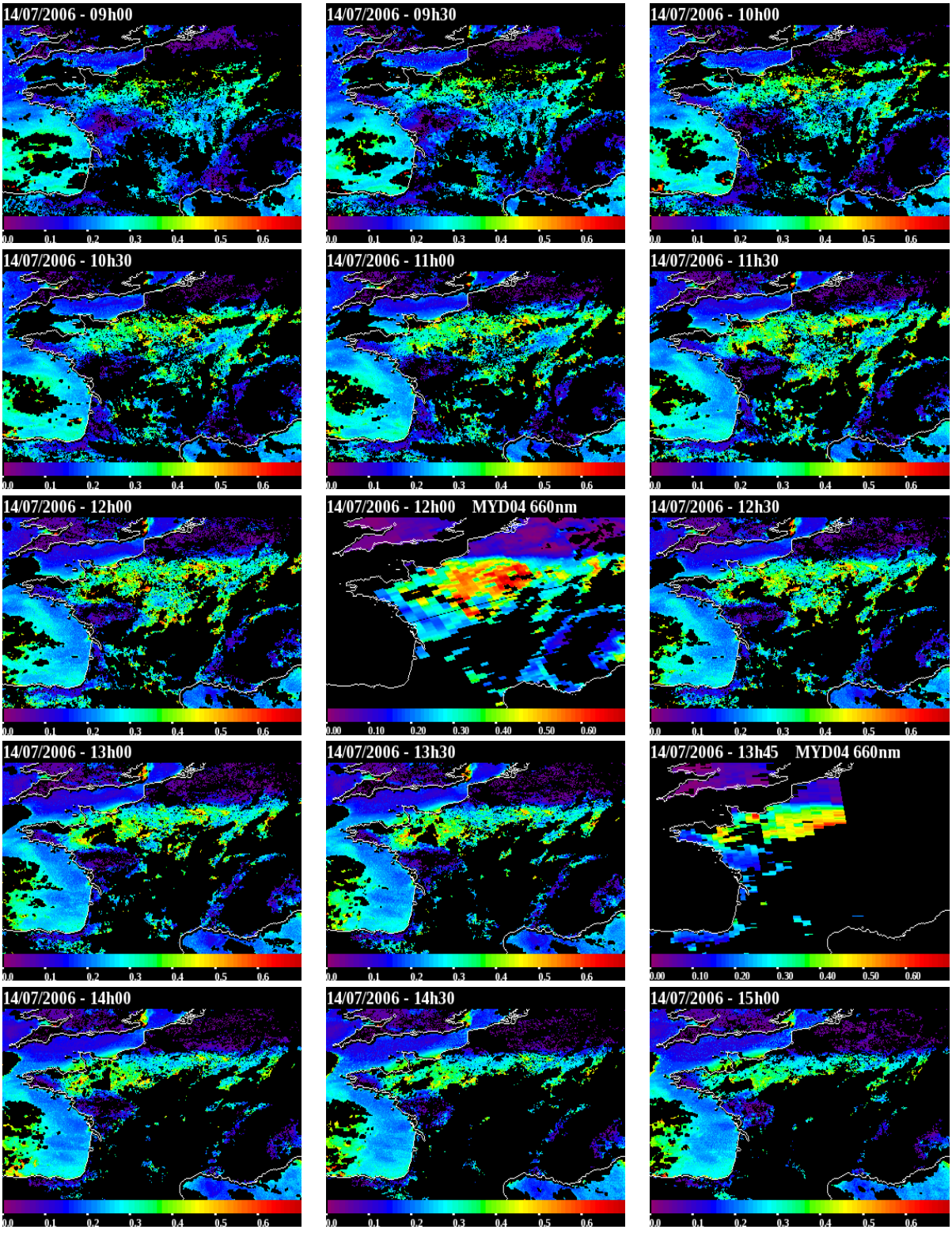

Fig. 8. Maps of aerosol optical thickness retrieved by SEVIRI at 0.6 µm for the 14 July 2006 above France, Benelux and West Germany from 09:00 to 15:00. Two MODIS AQUA aerosol optical thickness level 2 maps are also showed at 12:00 and 13:45. The color scale is from 0 to 0.7.

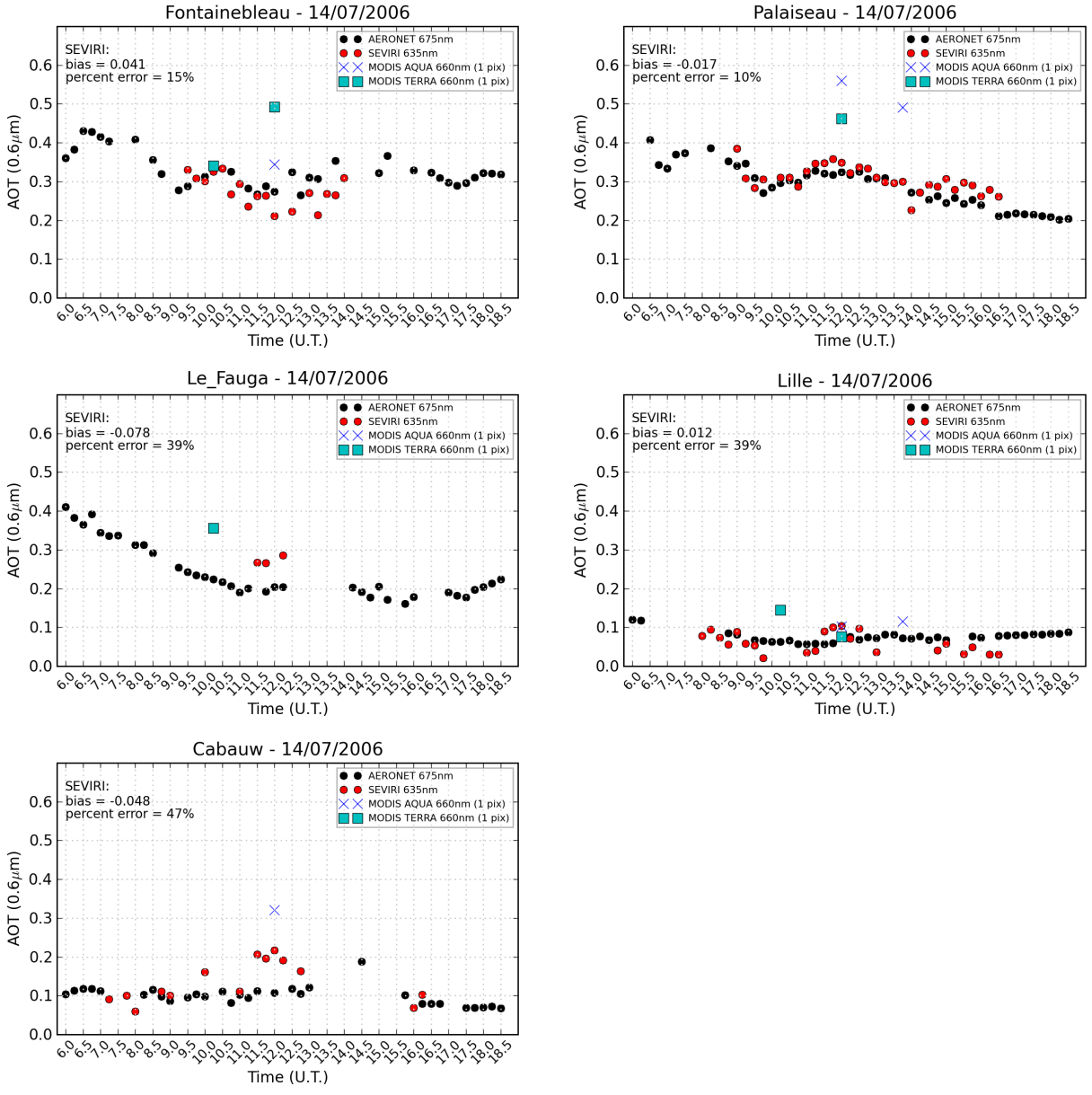

Fig. 9. Temporal evolution of the aerosol optical thickness above Fontainebleau, Palaiseau, Le Fauga (near Toulouse), Lille and Cabauw for the 14 July 2006. The black dots are AERONET, the red dots are SEVIRI and the blue crosses and cyan squares are for MODIS AQUA and TERRA at 660 nm. The mean bias and the mean relative bias between AERONET and SEVIRI are indicated on each plot. The SEVIRI and MODIS pixels are the ones geolocated with the AERONET station. The time scale is from 06:00 to 18:45 UTC and the AOT scale is from 0 to 0.7.

and 13:50 respectively have been aggregated to produce maps of AOT that can be directly compared to the SEVIRI derived aerosol product. MODIS AOT over land (Remer et al., 2005) is delivered at 660nm under the name "Corrected_Aerosol_Optical_Depth_Over_Land". We used the Quality Assurance (QA) index to filter pixels and keep only those with a QA = 3 as recommended by Levy et al. (2009b).

The comparison with MODIS confirms the presence of a large aerosol load over France and Germany. We can observe the same geographical patterns between maximum and minimum of aerosol load and clouds (black zones). MODIS seems to retrieve higher AOT over the region with AOT values between 0.2 and 0.6 for MODIS while they range from 0.05 to 0.5 for SEVIRI at 12:00 and 13:45. The differences could be due to the aerosol models used by the two algorithms or due to the surface reflectance estimation for

which both methods are different. Obviously, MODIS takes advantage of its higher spatial resolution (between 250 m and 1 km) and spectral coverage to better discriminate clouds and aerosols and MODIS aerosol products have demonstrated a very good correlation with AERONET measurements (Levy et al., 2007). However, where MODIS has only two daily observations at best for a given region, SEVIRI can follow the temporal evolution of the aerosol plume in a qualitative way as will be illustrated in the following Section.

These results illustrate that, despite residual contamination by clouds, SEVIRI allows for the monitoring of the daily AOT variability. Furthermore, Fig. 8 clearly illustrates that cloud coverage remains an issue for monitoring the spatial evolution of AOT. Contrary to other orbiting sensors, SEVIRI allows multiple observations per day which increase the probability of observing a given pixel under clear sky condition and further help in reducing cloud contamination when computing a daily mean value of AOT.

6 Observation of the diurnal variability

We compare here the temporal series of the aerosol optical thickness of the SEVIRI level 2 filtered product and the MODIS level 2 product onboard both platforms, Aqua and Terra, over the stations concerned by the aerosol event on the 14 July 2006 (Fig. 9).

Over Fontainebleau, the satellites data are coherent with the AERONET inversions, except for the Terra observations at 12:00, which over-estimate largely the AOT. We observe that SEVIRI under-estimates slightly the AERONET AOT while MODIS over-estimates these AOTs. SEVIRI observations are only available during midday due to the presence of clouds for SEVIRI and for obvious orbital reasons for MODIS. The slight variation of the AOT between 09:00 and 14:00 is not captured by MODIS while SEVIRI seems to observe this variation despite the temporal noise due to the retrieved aerosol model changing over the course of the day. Note however that the noise introduced by unstable model selection is still significantly lower than the difference between AERONET and the second MODIS/Terra retrieval.

Over Palaiseau, SEVIRI observes the variability of the aerosol load in very good agreement with AERONET measurements. MODIS over-estimates the aerosol optical thickness by 0.1 to 0.2. While errors can be introduced by the projection of the coarser resolution MODIS product in the SEVIRI grid, which can affect the absolute value of the AOT, MODIS has also difficulties to observe the diurnal variability whereas SEVIRI seems to perform very well for that purpose. The number of satellite retrievals is low over Le Fauga, and the values exceed the ground based measurements. Over Lille, a good correlation is found between both satellites and the AOT from AERONET. The advantage of SEVIRI observation is demonstrated once more with retrievals from 08:00 to 16:30, as can be observed also over Cabauw station. However, over-estimations of the AOT by MODIS and SEVIRI over this station are observed around midday.

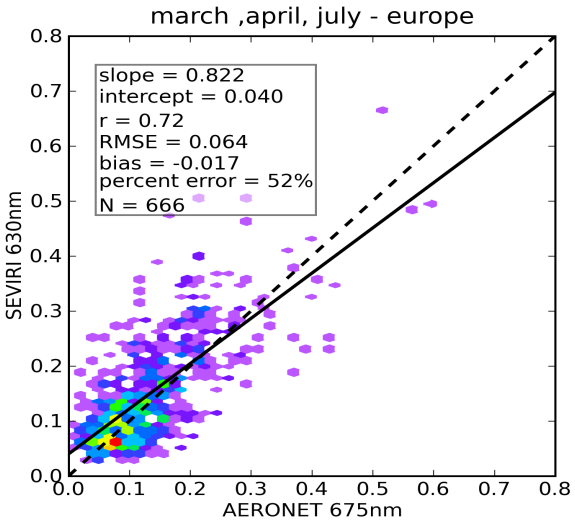

Fig. 10. Density graph of the daily SEVIRI and AERONET AOT at 0.6µm for European stations for the 3 months of interest (March, April and July 2006). The linear regression is plotted and the results of this regression are indicated on the graph.

Even if more comparisons between AERONET, SEVIRI and MODIS level 2 products have to be carried out to evaluate the real impact of a geostationary sensor compared to polar orbiting satellites, we demonstrate here that SEVIRI has a great potential to follow the diurnal evolution of atmospheric aerosol loading with a good accuracy.

7 Daily averaged product

7.1 AERONET comparison

The daily mean values are produced by accumulation of the valid retrievals for each day and the standard deviation is also computed.

The advantage of such a product is to minimize the temporal noise of SEVIRI AOT and also to have a better representation of the daily mean atmospheric turbidity by averaging individual retrievals and limiting cloud contamination.

A global linear regression is calculated between AERONET and SEVIRI daily AOT and the results, shown on Fig. 10, are similar to those obtained for the level 2 validation (see Sect. 4.3). The number of match-up is greater than 600 and the bias is the same as for the level 2 validation. Only the correlation coefficient increases significantly ($r = 0.72$).

Figure 11 shows the daily AOT over the 3 months of interest for 4 stations: Fontainebleau, Granada, Le Fauga and Rome. On April and July for the four stations and also for Fontainebleau in March, SEVIRI AOT product follows

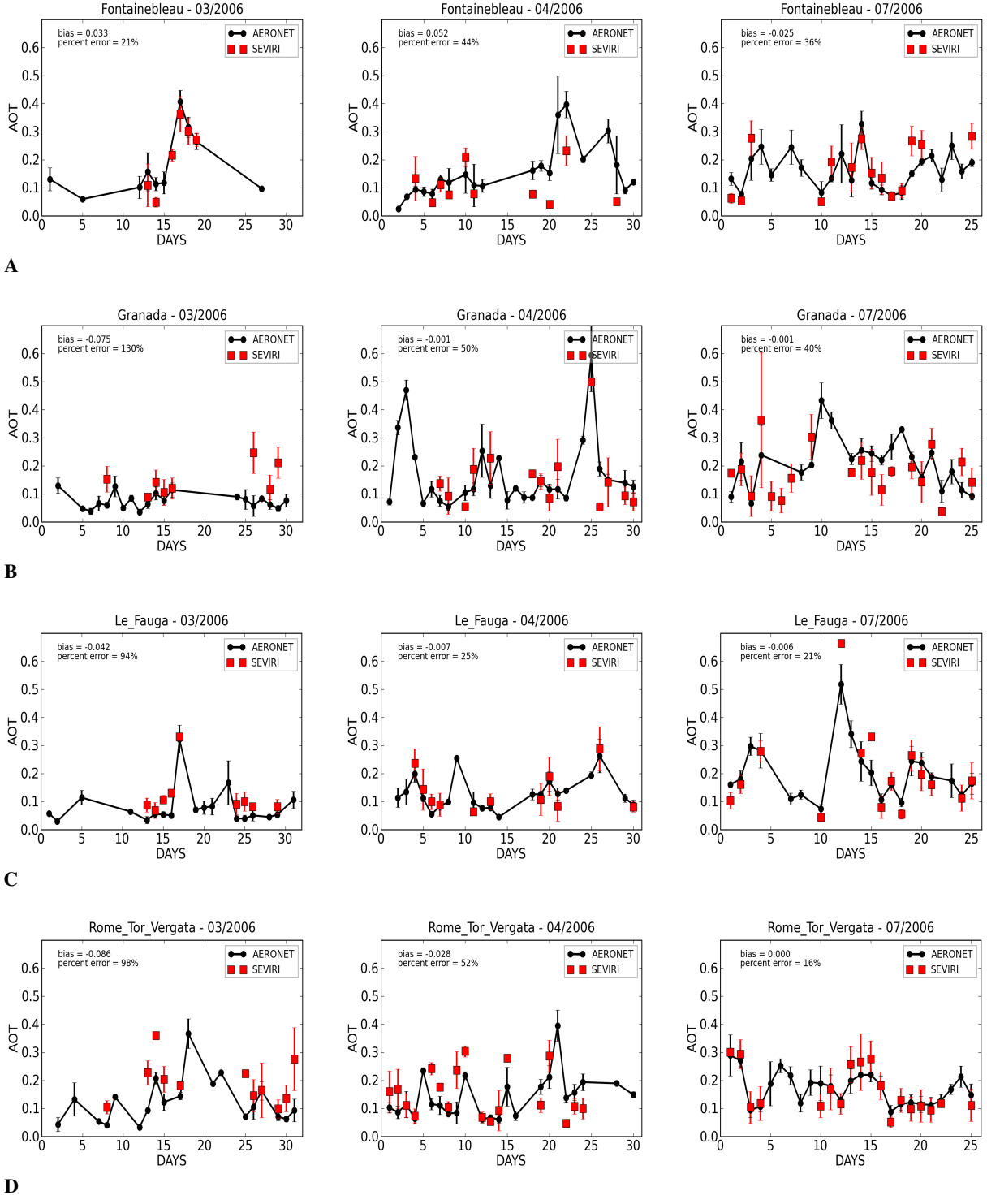

Fig. 11. Temporal evolution of the daily averaged AOT for 4 AERONET stations in March, April and July 2006. Stations are Fontainebleau **(A)**, Granada **(B)**, Le Fauga **(C)** and Rome Tor Vergata **(D)**. The black curve is the AOT AERONET and the red one is the AOT SEVIRI. The standard deviations are also plotted. The averages are made independently for AERONET and SEVIRI.

very well the AERONET measurements. The mean absolute relative error ranges from 16 % to 52 % between April and July and the biases are often close to zero with exceptions around 0.02 or 0.05. However, for 3 stations in March, Granada, Le Fauga and Rome, high relative errors appear ($\Delta\tau > 0.9\,\tau$) and biases are greater than 0.04. We can reasonably say that, even if some biases exist, daily SEVIRI AOTs in Fig. 11 correctly reproduce the monthly variability observed by AERONET.

On the 10 and the 11 July, Rome AERONET station measures an average AOT of 0.2 and 0.18. SEVIRI is very well correlated on the 11 but retrieves an AOT of 0.1 on the 10. An analysis at the original temporal resolution level 2 product shows that diurnal cycles are observed on these two days: AOT around 0.12–0.15 in the morning, and 0.22 to 0.3 in the afternoon (see Fig. 6). This could explain the difference between AERONET and SEVIRI daily mean AOT. On the 10, SEVIRI retrieves AOT only in the morning while in the afternoon values are discarded because they are declared as uncertain clear-sky pixels.

On 3 April 2006 for Granada, AERONET measures a daily AOT of 0.46 with only 2 measurements at 07:00 and 07:30 while SEVIRI has no retrieval because all the pixels are declared as cloudy. On 2 April 2006, in the afternoon, AERONET measures also high AOT ($\tau_{AER} = 0.33$) while SEVIRI retrieves AOT between 0.3 and 0.6 but all associated to uncertain clear-sky and thus discarded. That same situation occurs on 4 April 2006 where pixels with valid values are retrieved by SEVIRI but considered as doubtful (uncertain clear-sky) or cloudy.

These two examples again illustrate the importance of the cloud mask and the difficulty to avoid wrong identification between clear-sky and cloudy pixels.

For the four stations of interest, the average number of individual level 2 AOT values used to calculate a daily AOT is greater than 4. In March, this value reaches 5 for Le Fauga and Rome, and 8 for Fontainebleau and Granada. In July, this value is ranging from 7 (Fontainebleau) to 13 (Le Fauga and Rome). This SEVIRI product thus provides daily AOT which are much more representative than polar orbiting sensors such as MODIS which allows only two measurements per day at best. It is noteworthy that the number of individual AOT used to compute the daily mean from SEVIRI is usually comparable to that of AERONET.

Globally, SEVIRI AOT retrievals reflect very well the AOT measured by AERONET and allow a satisfactory monitoring of day to day aerosols variability.

7.2 Comparison with MODIS level 3 maps

We produced daily averaged maps from the SEVIRI level 2 filtered product and compared those maps with the MODIS Aqua level 3 daily AOT product at 0.6 µm (file type MYD08 and collection 051, Hubanks et al., 2008).

The original projection of MODIS is rectangular with a spatial resolution of 1°. The MODIS product chosen to compare with is the corrected and screened AOT in the 0.66 µm channel above land and the effective AOT above ocean. It is the most confident level 3 product available (Levy et al., 2009a) because it includes an averaged AOT weighted by the confidence index.

Our level 3 SEVIRI product has been projected on a rectangular grid with a resolution of 0.1° which is close to the original SEVIRI radiance data over Europe.

Figure 12 shows daily maps from 17 to 20 July 2006. These maps illustrate the main differences between the two products: MODIS allows to retrieve AOT at high latitudes where SEVIRI is limited by the viewing zenith angle (large air masses). However, SEVIRI maps are built from several original images during the day which increase the probability of retrieval for a given pixel and are not affected by the inter-orbital gaps like MODIS.

Another important feature shown in Fig. 12 is the very low level of noise in our SEVIRI product compared to that of MODIS, particularly around cloudy areas (e.g. over France and Spain on the 19 July on Fig. 12). This is due partly to the fact that our cloud mask is very restrictive but also because daily SEVIRI AOT are computed from several values retrieved during the day, which limits the impact of contaminated pixels.

For these 4 days an aerosol event coming from the North of Africa (17 July 2006) crosses Europe and reaches the North West of Europe on 20 July 2006. It is a frequent event that seasonal dust transport coming from the Sahara fly over the Mediterranean sea (Moulin et al., 1997). Both sensors allow to monitor very well this event.

On 17 July 2006, SEVIRI retrieves an AOT of 0.3 on the south west part of Spain and 0.1 over the rest of Europe while MODIS retrieves an AOT level of 0.35 all over Spain and 0.1 elsewhere. Over almost the whole Europe the number of level 2 SEVIRI pixels used to compute the daily average is greater than 5 and lower than 30 (Fig. 13). This number drops down below 5 only over a part of Spain and France. This again increases the confidence of the delivered daily averaged AOT product.

Outside of cloudy areas, MODIS and SEVIRI products are very similar over oceans. Over land, major differences appear even if the spatial patterns are globally similar. Part of the large apparent differences can be explained by the coarse resolution of the MODIS level 3 daily product and the fact that the level 2 to level 3 aggregation tends to overemphasize grid boxes for which very few pixels with large AOT retrievals were available. Although this problem is minor for the monthly statistics, the weight of such grid boxes in the level 3 daily is clearly overestimated in the present comparison. This problem is particularly evident when looking at Turkey and Greece. The SEVIRI product shows very localized areas with high AOT (0.3–0.4) which seem to

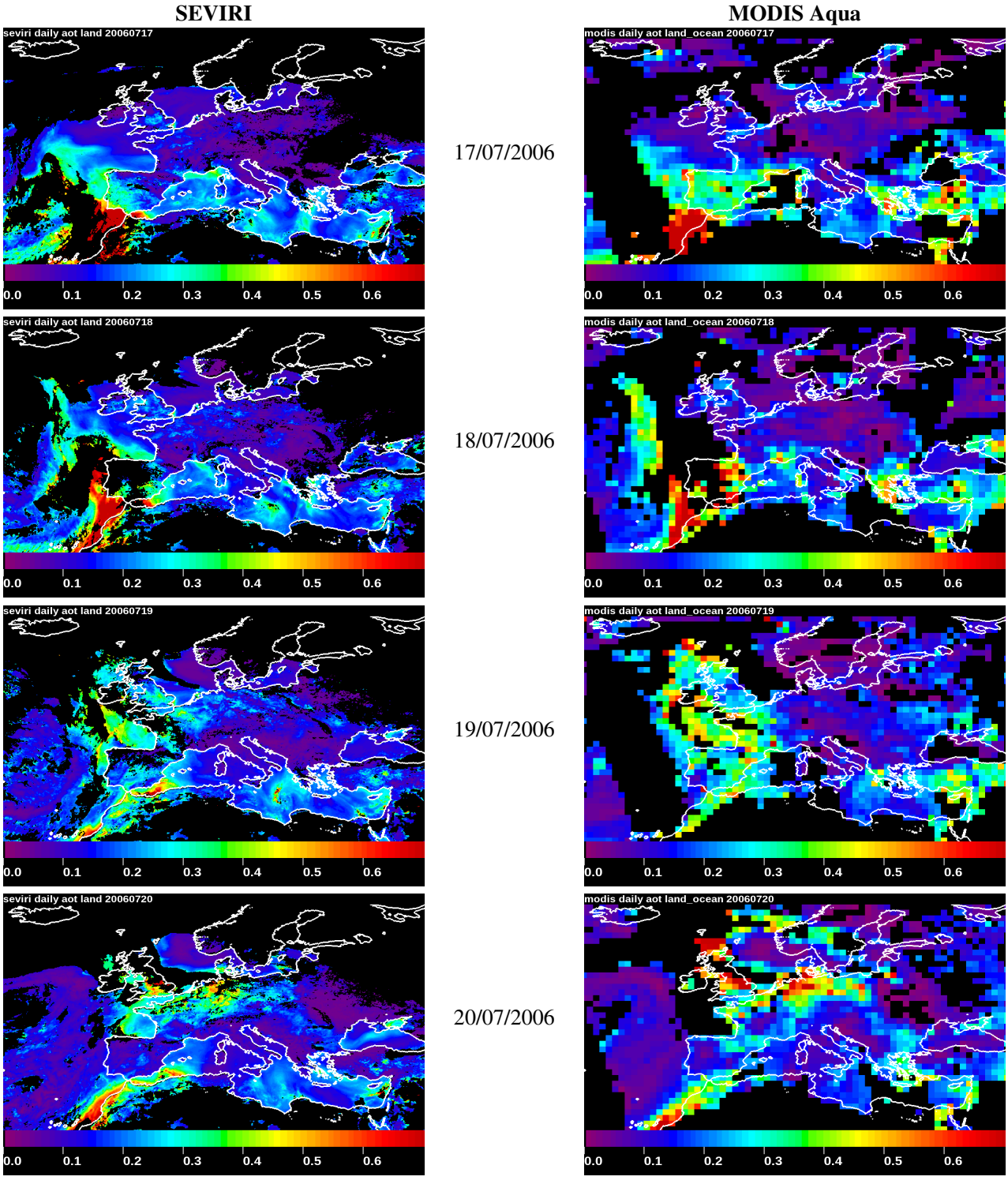

Fig. 12. Daily AOT maps at 0.6 µm above Europe for SEVIRI (left panel) and MODIS (right panel) sensors. The spatial resolution of SEVIRI is $0.1° \times 0.1°$ while it is $1°$ for MODIS. Days presented are from the 17 (top panel) to the 20 (bottom panel) July 2006. The color scale is from 0 to 0.7.

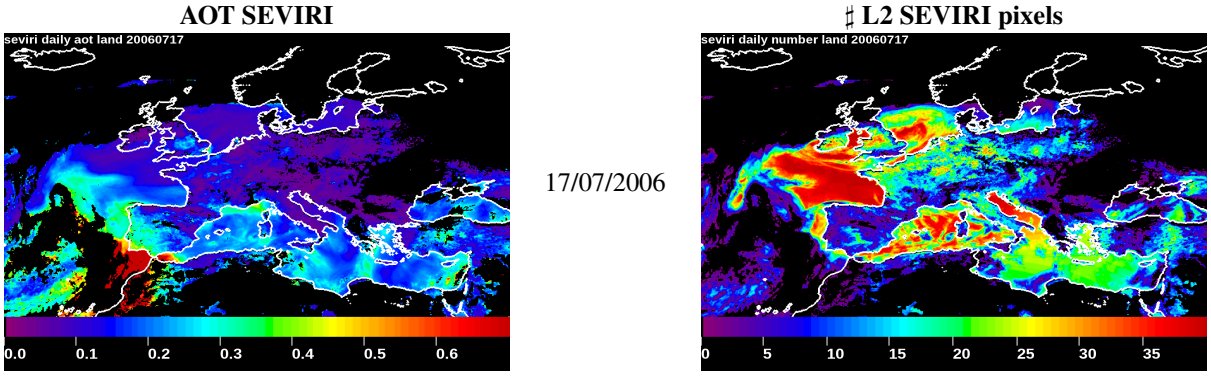

Fig. 13. Daily SEVIRI maps above Europe on the 17 July 2006: on the left the AOT at 0.6 µm and on the right the quantity of L2 pixels to process the AOT daily average.

significantly raise the mean AOT level over these countries in the MODIS product at 1° resolution.

8 Conclusions

We developed and implemented a method to retrieve the aerosol optical thickness at 0.6 µm over land using the SEVIRI data onboard MSG. This AOT product is delivered at the original SEVIRI spatial (3 km at nadir) and temporal resolution (15 min).

The algorithm has been developed for operational use within the French Data and Services Center for Cloud-Aerosol-Water-Radiation Interactions, ICARE (http://www.icare.univ-lille1.fr).

This paper is primarily intended to document the overall quality of a first revision of this AOT product that will be made publicly available through the ICARE data center. This first evaluation of the product quality was focused over Europe where retrievals are currently believed to have some virtues for the quantitative analysis of aerosol loading over land and its diurnal evolution.

The main assumption of the method is that the TOA reflectance increases with the aerosol reflectance in the VIS06 channel. This assumption is valid except above bright surfaces in the presence of absorbing aerosols. Then, to derive the surface reflectance in the VIS06 channel, we assume that over a period of 14 days the minimum of the Ozone and Rayleigh corrected TOA reflectance is the contribution of the surface reflectance and a residual aerosol background. By assuming that the aerosol background is low and equal to 0.03, we estimate the surface reflectance. This estimation of the surface reflectance also relies on the assumption that the properties of land do not change significantly during 14 days and that the solar angles (zenith and azimuthal) vary only slightly (from 1° to 4°).

The AOT at 0.6 µm is retrieved using Look-Up-Tables for 5 aerosol models. With the VIS08 and NIR16 channels, the best model is chosen by iteratively calculating the difference between measured and simulated reflectances at these two wavelengths.

The level 2 AOT product is filtered to avoid non-favorable geometrical configurations and cloud contamination in order to remove the maximum of spurious retrievals.

We compared this level 2 product with ground based AERONET measurements at 0.675 µm and validated the AOT above Europe for 3 months of 2006. The final set contains more than five thousand match-ups and the correlation is good between the two datasets ($r = 0.64$). SEVIRI tends to slightly over-estimate AOT compared to AERONET with a positive bias of 0.017. The relative error and the size of the sample decrease drastically between low and high AOT: 63 % for $\tau < 0.1$ with $N = 2557$ and less than 1 % for $\tau \geq 0.3$ with $N = 122$.

The correlation is better in July ($r = 0.7$) with a high number of retrievals ($N = 3291$) compared to the two other more cloudy months: April ($N = 1870$, $r = 0.54$) and March ($N = 476$, $r = 0.49$).

Differences observed and discussed here between SEVIRI, MODIS and AERONET AOT could also partly be caused by calibration issues with SEVIRI channels. Different validation studies of the 0.6 µm channel calibration coefficient (Ham and Sohn, 2010; Doelling et al., 2004; Jolivet et al., 2009) have found similar results pointing to a same value of about 6–7 % low bias for Meteosat-8. A simple sensitivity test demonstrated (not shown here) a clear impact of calibration on our product. Taking into account the calibration correction on SEVIRI radiances, allowed us to improve the linear regression coefficient on one hand but deteriorated the bias and relative error on the other hand. Degradation of the relative error and dispersion could be a consequence of inconsistent calibration between the various channels if only the 0.6 µm channel is corrected. Therefore, it is critical for the future that improved and consistent calibration coefficients of the visible and near infrared channels be made available. At this stage we preferred to keep the

official coefficients delivered by EUMETSAT to prevent introduction of additional problems due to inconsistent intercalibration of SEVIRI channels. Clearly, there is ample space for improvement on this side.

A temporal comparison shows very good results and demonstrates that SEVIRI is able to successfully monitor the aerosol load during the day. With a number of retrievals per day greater than 5, the diurnal cycle of aerosol is also observable. The possibility to follow local or regional aerosol features on a 15 minutes timescale is illustrated over Europe.

The monitoring of aerosol load over long periods using a daily mean AOT is also possible according to the comparison with the daily AOT AERONET reference measurements. Moreover, qualitative comparisons with the MODIS level 3 daily product show general consistency between SEVIRI and MODIS over the Europe during an aerosol event coming from the North of Africa and crossing Europe during several days in July 2006. The SEVIRI product also proved suitable for local and regional studies. In addition, direct comparisons with AERONET retrievals and MODIS level 2 products demonstrate that our algorithm perform very well and sometimes better than MODIS while capturing the diurnal variability of aerosol load in a qualitative way that is inaccessible to polar orbiting sensors such as MODIS.

It must be acknowledged that our AOT SEVIRI product currently suffers from some drawbacks due to difficulties in cloud masking related to the spatial resolution of SEVIRI (from 3 to 5 km) which does not allow to detect small scale clouds. However, cloud mask in remote sensing of aerosols results from a compromise and requires a permanent effort for improvement (Kaufman et al., 2005; Frey et al., 2008; Saunders and Kriebel, 1988; Heidinger et al., 2002; Simpson et al., 2001; Trishchenko and Radkevich, 2009; Huo and Lu, 2009; Hagolle et al., 2005).

Another inherent weakness of our algorithm is the difficulty to properly estimate the surface reflectance in specific conditions. This is the case for desert surfaces as well as in specific geometric conditions over vegetation ("hot spot" configuration). Solving these problems would require additional constraints on BRDF from theoretical models (e.g. Roujean et al., 1992) or from other sensors such as MODIS or POLDER onboard LEO satellites. Besides, methods based on IR channels to retrieve an aerosol product over bright surfaces exist (Legrand and N'doumé, 2001; De Paepe and Dewitte, 2009). These could, in combination with our product, contribute to a better monitoring of aerosols from geostationary satellites.

Also, the assumed aerosol background is probably underestimated over regions with significant permanent aerosol loads. The use of LEO satellites data to improve estimation of the residual on the day used for the reference is currently being explored.

The high temporal resolution of the SEVIRI product presented in this paper is useful for the study of aerosol plumes at different time-scales (an hour, a half day) and could find applications for Earth radiation budget studies (De Paepe et al., 2008) and for air quality monitoring (Sifakis, 1998; Health Effects Institute, 2000) for instance through data assimilation in regional aerosol models.

Acknowledgements. The authors are grateful to EUMETSAT for providing SEVIRI/MSG data, NASA for making available MODIS products as well as AERONET PIs and their staff for establishing and maintaining the sites used in this investigation. The authors are also thankful to CNES agency and the Association Nationale de la Recherche et de la Technologie for financial support of these studies. Finally, we would like to thank very much P.-Y. Deschamps for his inspiring ideas and constructive comments throughout these studies.

Edited by: P. Stammes

The publication of this article is financed by CNRS-INSU.

References

Ackerman, S. A., Strabala, K. I., Menzel, W. P., Frey, R. A., Moeller, C. C., and Gumley, L. E.: Discriminating Clear-sky from Clouds with MODIS, J. Geophys. Res., 103, 32141–32157, 1998.

Albrecht, B.: Aerosols, Cloud Microphysics and Fractional Cloudiness, Science, 245, 1227–1230, 1989.

Bernard, E., Ramon, D., Jolivet, D., Moulin, C., Riedi, J., Deschamps, P.-Y., Nicolas, J.-M., and Hagolle, O.: Aerosol retrieval over land in the 635 nm channel of MSG/SEVIRI sensor: a hourly and daily AOT product above Europe, in: Eumetsat Meteorological Satellite Conference, 2009.

Carrer, D., Roujean, J., Hautecoeur, O., and Elias, T.: Daily estimates of aerosol optical thickness over land surface based on a directional and temporal analysis of SEVIRI MSG visible observations, J. Geophys. Res., 115, D10208, doi:10.1029/2009JD012272, 2010.

Charlson, R., Lovelock, J., Andreae, M., and Warren, S.: Oceanic phytoplankton, atmospheric sulfur,cloud albedo and climate, Nature, 326, 655–661, 1987.

Charlson, R. J., Schwartz, S. E., Hales, J. M., Cess, R. D., Coakley, J. A., Hansen, J. E., and Hofmann, D. J.: Climate Forcing by Anthropogenic Aerosols, Science, 255, 423–430, doi:10.1126/science.255.5043.423, 1992.

Chu, D. A., Kaufman, Y. J., Zibordi, G., Chern, J. D., Mao, J., Li, C., and Holben, B. N.: Global monitoring of air pollution over land from the Earth Observing System-Terra Moderate Resolution Imaging Spectroradiometer (MODIS), J. Geophys. Res., 108, 4661, doi:10.1029/2002JD003179, 2003.

Crutzen, P., Ramanathan, V., Anderson, T., Charlson, R., Schwartz, S., Knutti, R., Boucher, O., Rodhe, H., and Heintzenberg, J.: The Parasol effect on climate, Science, 302, 1679–1681, 2003.

De Paepe, B. D., Ignatov, A., Dewitte, S., and Ipe, A.: Aerosol retrieval over ocean from SEVIRI for the use in GERB Earth's radiation budget analyses, Remote Sens. Environ., 112, 2455–2468, 2008.

De Paepe, B. and Dewitte, S.: Dust Aerosol Optical Depth Retrieval over a Desert Surface Using the SEVIRI Window Channels, J. Atmos. Ocean. Tech., 26, 704–718, doi:10.1175/2008JTECHA1109.1, 2009.

Denman, K. L., Brasseur, G., Chidthaisong, A., Ciais, P., Cox, P. M., Dickinson, R. E., Hauglustaine, D., Heinze, C., Holland, E., Jacob, D., Lohmann, U., Ramachandran, S., da Silva Dias, P. L., Wofsy, S. C., and Zhang, X.: Couplings Between Changes in the Climate System and Biogeochemistry, in: Climate Change 2007: The Physical Science Basis. Contribution of Working Group I to the Fourth Assessment Report of the Intergovernmental Panel on Climate Change, edited by: Solomon, S., Qin, D., Manning, M., Chen, Z., Marquis, M., Averyt, K. B., Tignor, M., and Miller, H. L., Cambridge University Press, Cambridge, UK and New York, NY, USA, 2007.

Doelling, D., Nguyen, L., and Minnis, P.: Calibration comparisons between SEVIRI, MODIS, and GOES data, in: Eumetsat Meteorological Satellite Conference, 77–83, 2004.

Emili, E., Popp, C., Petitta, M., Riffler, M., Wunderle, S., and Zebisch, M.: PM_{10} remote sensing from geostationary SEVIRI and polar-orbiting MODIS sensors over the complex terrain of the European Alpine region, Remote Sens. Environ., 114, 2485–2499, doi:10.1016/j.rse.2010.05.024, 2010.

EUMETSAT: Radiometric Calibration of MSG SEVIRI Level 1.5 Image Data in Equivalence Spectral Blackbody Radiance, technical document number EUM/OPS-MSG/TEN/03/0064, 2007.

Forster, P., Ramaswamy, V., Artaxo, P., Berntsen, T., Betts, R., Fahey, D. W., Haywood, J., Lean, J., Lowe, D. C., Myhre, G., Nganga, J., Prinn, R., Raga, G., Schulz, M., and Van Dorland, R.: Changes in Atmospheric Constituents and in Radiative Forcing, in: Climate Change 2007: The Physical Science Basis. Contribution of Working Group I to the Fourth Assessment Report of the Intergovernmental Panel on Climate Change, edited by: Solomon, S., Qin, D., Manning, M., Chen, Z., Marquis, M., Averyt, K. B., Tignor, M., and Miller, H. L., Cambridge University Press, Cambridge, UK and New York, NY, USA, 2007.

Fraser, R. S. and Kaufman, Y. J.: The relative importance of aerosol scattering and absorption in remote-sensing, IEEE T. Geosci. Remote, 23, 625–633, 1985.

Frey, R. A., Ackerman, S. A., Liu, Y., Strabala, K. I., Zhang, H., Key, J. R., and Wang, X.: Cloud Detection with MODIS. Part I: Improvements in the MODIS Cloud Mask for Collection 5, J. Atmos. Ocean. Tech., 25, 1057–1072, doi:10.1175/2008JTECHA1052.1, 2008.

Ghan, S., Laulainen, N., Easter, R., Wagener, R., Nemesure, S., Chapman, E., Zhang, Y., and Leung, R.: Evaluation of aerosol direct radiative forcing in MIRAGE, J. Geophys. Res., 106, 5295–5316, doi:10.1029/2000JD900502, 2001.

Govaerts, Y. and Clerici, M.: MSG-1/SEVIRI Solar Channels Calibration Commissionning Activity Report, EUMETSAT, EUM/MSG/TEN/04/0024, 2004.

Govaerts, Y. M., Wagner, S., Lattanzio, A., and Watts, P.: Joint retrieval of surface reflectance and aerosol optical depth from MSG/SEVIRI observations with an optimal estimation approach: 1. Theory, J. Geophys. Res., 115, D02203, doi:10.1029/2009JD011779, 2010.

Grosso, N., Ferreira, F., and Mesquita, S.: Chapter 3.1 Improvement in particles (PM_{10}) urban air quality mapping interpolation using remote sensing data, in: Air Pollution Modeling and Its Application XVIII, edited by: Borrego, C. and Renner, E., vol. 6 of Developments in Environmental Sciences, Elsevier, 265–274, doi:10.1016/S1474-8177(07)06031-7, 2007.

Guerrieri, L., Corradini, S., Pugnaghi, S., and Santangelo, R.: An aerosol optical thickness retrieval algorithm for Meteosat Second Generation (MSG) data over land: applications to the Mediterranean area, in: Society of Photo-Optical Instrumentation Engineers (SPIE) Conference Series, vol. 6745, 2007.

Hagolle, O., Lobo, A., Maisongrande, P., Cabot, F., Duchemin, B., and Pereyra, A. D.: Quality assessment and improvement of temporally composited products of remotely sensed imagery by combination of VEGETATION 1 and 2 images, Remote Sens. Environ., 94, 172–186, doi:10.1016/j.rse.2004.09.008, 2005.

Ham, S.-H. and Sohn, B. J.: Assessment of the calibration performance of satellite visible channels using cloud targets: application to Meteosat-8/9 and MTSAT-1R, Atmos. Chem. Phys., 10, 11131–11149, doi:10.5194/acp-10-11131-2010, 2010.

Hansen, J., Sato, M., and Ruedy, R.: Radiative forcing and climate response, J. Geophys. Res., 102, 6831–6864, doi:10.1029/96JD03436, 1997.

Hansen, J., Sato, M., Ruedy, R., Lacis, A., and Oinas, V.: Global warming in the twenty-first century: An alternative scenario, vol. 97, The National Academy of Sciences, 9875–9880, 2000.

Haywood, J. and Boucher, O.: Estimates of the direct and indirect radiative forcing due to tropospheric aerosols: A review, Rev. Geophys., 38, 513–543, doi:10.1029/1999RG000078, 2000.

Health Effects Institute: Reanalysis of the Harvard Six Cities Study and the American Cancer Society Study of Particulate Air Pollution and Mortality: A Special Report of the Intitute's Particle Epidemiology Reanalysis Project, Cambridge MA, Health Effects Institute, 2000.

Hegg, D. A., Ferek, R. J., and Hobbs, P. V.: Light scattering and cloud condensation nucleus activity of sulfate over the Northeast Atlantic Ocean, J. Geophys. Res., 98, 14887–14894, doi:10.1029/93JD01615, 1993.

Heidinger, A. K., Anne, V. R., and Dean, C.: Using MODIS to Estimate Cloud Contamination of the AVHRR Data Record, J. Atmos. Ocean. Tech., 19, 586–601, doi:10.1175/1520-0426(2002)019<0586:UMTECC>2.0.CO;2, 2002.

Holben, B. N., Eck, T. F., Slutsker, I., Tanré, D., Buis, J. P., Setzer, A., Vermote, E., Reagan, J. A., Kaufman, Y. J., Nakajima, T., Lavenu, F., Jankowiak, I., and Smirnov, A.: AERONET – A Federated Instrument Network and Data Archive for Aerosol Characterization, Remote Sens. Environ., 66, 1–16, 1998.

Hubanks, P. A., King, M. D., Platnick, S., and Pincus, R.: MODIS Atmospheric L3 gridded product: Algorithm Theoretical Basis Document, 2008.

Huo, J. and Lu, D.: Cloud Determination of All-Sky Images under Low-Visibility Conditions, J. Atmos. Ocean. Tech., 26, 2172–2181, doi:10.1175/2009JTECHA1324.1, 2009.

Jolivet, D., Ramon, D., Riedi, J., and Roebeling, R.: Aerosol retrievals from METEOSAT-8, SAF on Climate Monitoring, Visiting Scientist Report, 2006.

Jolivet, D., Nicolas, J.-M., Bernard, E., Deschamps, P.-Y., and Ramon, D.: In-flight calibration of SEVIRI solar channels on board MSG platforms, in: Eumetsat Meteorological Satellite Conference, Bath, UK, 21–25 September 2009.

Junge, C. E.: Atmospheric Chemistry, vol. 4 of Advances in Geophysics, Elsevier, 1–108, doi:10.1016/S0065-2687(08)60484-7, 1958.

Kaufman, Y. J., Tanré, D., Remer, L. A., Vermote, E. F., Chu, A., and Holben, B. N.: Operational remote sensing of tropospheric aerosol over land from EPS moderate resolution imaging spectroradiometer, J. Geophys. Res., 102, 17051–17067, 1997.

Kaufman, Y. J., Tanré, D., and Boucher, O.: A satellite view of aerosols in the climate system, Nature, 419, 215–223, 2002.

Kaufman, Y. J., Remer, L. A., Tanré, D., Li, R., Kleidman, R., Mattoo, S., Levy, R. C., Eck, T. F., Holben, B. N., Ichoku, C., Martins, J. V., and Koren, I.: A Critical Examination of the Residual Cloud Contamination and Diurnal Sampling Effects on MODIS Estimates of Aerosol Over Ocean, IEEE T. Geosci. Remote, 43, 2886–2897, doi:10.1109/TGRS.2005.858430, 2005.

Kettle, A. J. and Andreae, M. O.: Flux of dimethylsulfide from the oceans: a comparison of updated data sets and flux models, J. Geophys. Res., 105, 26793–26808, 2000.

King, M. D., Kaufman, Y. J., Tanré, D., and Nakajima, T.: Remote sensing of tropospheric aerosols from space: Past, Present and Future, B. Am. Meteorol. Soc., 80, 2229–2259, 1999.

Knapp, K. R.: Quantification of aerosol signal in GOES 8 visible imagery over the United States, J. Geophys. Res., 107, 4426, doi:10.1029/2001JD002001, 2002.

Knapp, K. R., Vonder Haar, T. H., and Kaufman, Y. J.: Aerosol optical depth retrieval from GOES-8: Uncertainty study and retrieval validation over South America, J. Geophys. Res., 107, 4055–4067, 2002.

Knapp, K. R., Frouin, R., Kondragunta, S., and Prados, A.: Toward aerosol optical depth retrievals over land from GOES visible radiances: determining surface reflectance, Int. J. Remote Sens., 26, 4097–4116, 2005.

Koelemeijer, R. B. A., Homan, C. D., and Matthijsen, J.: Comparison of spatial and temporal variations of aerosol optical thickness and particulate matter over Europe, Atmos. Environ., 40, 5304–5315, doi:10.1016/j.atmosenv.2006.04.044, 2006.

Legrand, M. and N'doumé, C.: Satellite detection of dust using the IR imagery of Meteosat: 1. Infrared difference dust index, J. Geophys. Res., 106, 18251–18274, doi:10.1029/2000JD900749, 2001.

Lenoble, J. and Brogniez, C.: A comparative review of radiation aerosol models, Beitraege zur Physik der Atmosphaere (ISSN 0005-8173), 57, 1–20, 1984.

Lenoble, J., Herman, M., Deuze, J. L., Lafrance, B., Santer, R., and Tanré, D.: A successive order of scattering code for solving the vector equation of transfer in the earth's atmosphere with aerosols, J. Quant. Spectosc. Ra., 107, 479–507, 2007.

Levy, R. C., Remer, L. A., Mattoo, S., Vermote, E. F., and Kaufman, Y. J.: Second-generation operational algorithm: Retrieval of aerosol properties over land from inversion of Moderate Resolution Imaging Spectroradiometer spectral reflectance, J. Geophys. Res., 112, D13211, doi:10.1029/2006JD007811, 2007.

Levy, R. C., Leptoukh, G. G., Kahn, R., Zubko, V., Gopalan, A., and Remer, L. A.: A Critical Look at Deriving Monthly Aerosol Optical Depth From Satellite Data, IEEE T. Geosci. Remote, 47, 2942–2956, doi:10.1109/TGRS.2009.2013842, 2009a.

Levy, R. C., Remer, L. A., Tanré, D., Mattoo, S., and Kaufman, Y. J.: Algorithm for remote sensing of tropospheric aerosol over dark targets from MODIS: Collections 005 and 051: Revision 2, ATBD, 2009b.

Lim, H. S., MatJafri, M. Z., and Abdullah, K.: Retrieval of Air Quality using a newly simulated algorithm from aerosol optical depth, Map Asia Conference, 2004.

Lohmann, U. and Feichter, J.: Global indirect aerosol effects: a review, Atmos. Chem. Phys., 5, 715–737, doi:10.5194/acp-5-715-2005, 2005.

Lohmann, U., Rotstayn, L., Storelvmo, T., Jones, A., Menon, S., Quaas, J., Ekman, A. M. L., Koch, D., and Ruedy, R.: Total aerosol effect: radiative forcing or radiative flux perturbation?, Atmos. Chem. Phys., 10, 3235–3246, doi:10.5194/acp-10-3235-2010, 2010.

Mishchenko, M. I., Geogdzhayev, I. V., Cairns, B., Carlson, B. E., Chowdhary, J., Lacis, A. A., Liu, L., Rossow, W. B., and Travis, L. D.: Past, present, and future of global aerosol climatologies derived from satellite observations: A perspective, J. Quant. Spectrosc. Ra., 106, 325–347, doi:10.1016/j.jqsrt.2007.01.007, 2007.

Moulin, C., Lambert, C. E., Dulac, F., and Dayan, U.: Control of atmospheric export of dust from North Africa by the North Atlantic Oscillation, Nature, 387, 691–694, 1997.

Muller, J.: MSG Level 1.5 Image Data Description, EUMETSAT, technical document number EUM/MSG/ICD/105, 2007.

Omar, A. H., Won, J., Winker, D. M., Yoon, S., Dubovik, O., and McCormick, M. P.: Development of global aerosol models using cluster analysis of Aerosol Robotic Network (AERONET) measurements, J. Geophys. Res., 110, D10S14, doi:10.1029/2004JD004874, 2005.

Platnick, S., King, M. D., Ackerman, S. A., Menzel, W. P., Baum, B. A., Riedi, J. C., and Frey, R. A.: The MODIS cloud products: algorithms and examples from Terra, IEEE T. Geosci. Remote, 41, 459–473, doi:10.1109/TGRS.2002.808301, 2003.

Popp, C., Hausser, A., Foppa, N., and Wunderle, S.: Remote sensing of aerosol optical depth over central Europe from MSG-SEVIRI data and accuracy assesment with ground-based AERONET measurements, J. Geophys. Res., 112, D24S11, doi:10.1029/2007JD008423, 2007.

Quaas, J., Boucher, O., Bellouin, N., and Kinne, S.: Satellite-based estimate of the direct and indirect aerosol climate forcing, J. Geophys. Res., 113, D05204, doi:10.1029/2007JD008962, 2008.

Ramon, D. and Santer, R.: Operational Remote Sensing of Aerosols over Land to Account for Directional Effects, Appl. Optics, 40, 3060–3075, 2001.

Remer, A. L., Kaufman, Y. J., Tanré, D., Matoo, S., Chu, D. A., Martins, J. V., Li, R. R., Ichoku, C., Levy, R. C., Kleidman, R. G., Eck, T. F., Vermote, E., and Holben, B. N.: The MODIS Aerosol Algorithm, Products and Validation, J. Atmos. Sci., 62, 947–973, 2005.

Roebeling, R. A., Deneke, H. M., and Feijt, A. J.: Validation of Cloud Liquid Water Path Retrievals from SEVIRI Using One Year of CloudNET Observations, J. Appl. Meteorol. Clim., 47, 206–222, 2008.

Rohen, G. J., von Hoyningen-Huene, W., Kokhanovsky, A., Dinter, T., Vountas, M., and Burrows, J. P.: Retrieval of aerosol mass load (PM_{10}) from MERIS/Envisat top of atmosphere spectral reflectance measurements over Germany, Atmos. Meas. Tech., 4, 523–534, doi:10.5194/amt-4-523-2011, 2011.

Roujean, J.-L., Leroy, M., and Deschamps, P.-Y.: A Bidirectional Reflectances Model of the Earth's Surface for the Correction of Remote Sensing Data, J. Geophys. Res., 97, 20455–20468, 1992.

Santer, J. R., Carrere, V., and Dubuisson, P.: Atmospheric correction over land for MERIS, Int. J. Remote Sens., 20, 1819–1840, 1999.

Saunders, R. W. and Kriebel, K. T.: An improved method for detecting clear sky and cloudy radiances from AVHRR data, Int. J. Remote Sens., 9, 123–150, doi:10.1080/01431168808954841, 1988.

Schulz, M., Textor, C., Kinne, S., Balkanski, Y., Bauer, S., Berntsen, T., Berglen, T., Boucher, O., Dentener, F., Guibert, S., Isaksen, I. S. A., Iversen, T., Koch, D., Kirkevåg, A., Liu, X., Montanaro, V., Myhre, G., Penner, J. E., Pitari, G., Reddy, S., Seland, Ø., Stier, P., and Takemura, T.: Radiative forcing by aerosols as derived from the AeroCom present-day and pre-industrial simulations, Atmos. Chem. Phys., 6, 5225–5246, doi:10.5194/acp-6-5225-2006, 2006.

Schwartz, S. E. and Slingo, A.: Enhanced shortwave cloud radiative forcing due to anthropogenic aerosols, NASA STI/Recon Technical Report N, 95, 34214–34261, 1995.

Seinfeld, J. H. and Pandis, S. N.: Atmospheric chemistry and physics, From air pollution to climate change, John Wiley and Sons, New York, 1997.

Sifakis, N. I.: Quantitative mapping of air pollution density using Earth observations: a new processing method and application to an urban area, Int. J. Remote Sens., 19, 3289–3300, doi:10.1080/014311698213975, 1998.

Simpson, J., McIntire, T., Stitt, J., and Hufford, G.: Improved cloud detection in AVHRR daytime and nighttime scenes over the ocean, in: Society of Photo-Optical Instrumentation Engineers (SPIE) Conference Series, edited by: Russell, J. E., Schaefer, K., and Lado-Bordowsky, O., vol. 4168, 48–55, 2001.

Thieuleux, F., Moulin, C., Bréon, F. M., Maignan, F., Poitou, J., and Tanré, D.: Remote sensing of aerosols over the oceans using MSG/SEVIRI imagery, Ann. Geophys., 23, 3561–3568, doi:10.5194/angeo-23-3561-2005, 2005.

Trishchenko, A. P. and Radkevich, A. V.: Improving the Cloud Mask For MERIS/ENVISAT Imagery Received Over Canada, AGU Fall Meeting Abstracts, F289+ pp., 2009.

Twomey, S.: Aerosols, clouds and radiation, Atmos. Environ., 25, 2435–2442, 1991.

Vermote, E., Tanré, D., Deuze, J.-L., Herman, M., and Morcrette, J. J.: Second Simulation of the Satellite in the Solar Spectrum, 6S: An overview, IEEE T. Geosci. Remote, 35, 675–686, 1997a.

Vermote, E. F., El Saleous, N., Justice, C. O., Kaufman, Y. J., Privette, J. L., Remer, L., Roger, J. C., and Tanré, D.: Atmospheric correction of visible to middle-infrared EOS-MODIS data over land surfaces: Background, operational algorithm and validation, J. Geophys. Res., 102, 17131–17142, doi:10.1029/97JD00201, 1997b.

Wagner, S. C., Govaerts, Y. M., and Lattanzio, A.: Joint retrieval of surface reflectance and aerosol optical depth from MSG/SEVIRI observations with an optimal estimation approach: 2. Implementation and evaluation, J. Geophys. Res., 115, D02204, doi:10.1029/2009JD011780, 2010.

Wang, J. and Christopher, S. A.: Intercomparison between satellite-derived aerosol optical thickness and $PM_{2.5}$ mass: Implications for air quality studies, Geophys. Res. Lett., 30, 2095, doi:10.1029/2003GL018174, 2003.

Wayne, R.: An Introduction to the Chemistry of the Atmospheres of Earth, the Planets, and their Satellites, Oxford University Press, Oxford, 2000.

Whitby, K.: Physical characterization of aerosol, in: Methods and standards for Environmental measurement, Proceedings of 8th IMR Symposium, 165–173, 1976.